The Dissertation Committee for Christina Marie Ragain Certifies that this is the approved version of the following dissertation:

Role of Local Electrostatic Fields in Protein-Protein and Protein-Solvent Interactions Determined by Vibrational Stark Effect Spectroscopy

Committee:

Lauren J. Webb, Supervisor

David A. Vanden Bout

Sean T. Roberts

Adrian T. Keatinge-Clay

Pengyu Ren

Role of Local Electrostatic Fields in Protein-Protein and Protein-Solvent Interactions Determined by Vibrational Stark Effect Spectroscopy

by

Christina Marie Ragain, B.S., M.S.

Dissertation

Presented to the Faculty of the Graduate School of

The University of Texas at Austin

in Partial Fulfillment

of the Requirements

for the Degree of

Doctor of Philosophy

The University of Texas at Austin

May 2014

Dedication

To my wonderful husband, Parker, and my beautiful daughter, Larissa. Thank you very much for all of your support and for going through this process with me. To my mom and dad, for supporting me and instilling me with the love of learning. I love you.

Acknowledgements

I would like to thank many people at The University of Texas at Austin especially in the Department of Chemistry for their support and for the opportunity to study.

I would like to thank Dr. Lauren J. Webb, my academic advisor, for her support and guidance during this process. Working with Dr. Webb for the past few years has given me the tools and opportunity to grow as a scientist and reach personal goals for my family and myself. I wish her all the best in future endeavors.

I would also like to thank the members of my doctoral committee: Dr. David Vanden Bout, Dr. Sean Roberts, Dr. Adrian Keatinge-Clay and Dr. Pengyu Ren for their support during my time at The University of Texas at Austin.

I worked directly with many people to create the work presented in this dissertation. Andrew Ritchie, thank you for collaborating with me on molecular dynamics research. Several bright and talented undergraduates and interns also worked on these projects. Thank you: Robert Newberry, Nancy Gonzalez, Juana Rivas, Coriyon Arrington and Meg Jameson. Thank you to the members of the Webb Group: Annette Raigoza, David Walker, Andrew Ritchie, Jason Dugger, Kjell Schroder, Rebika Shrestha, Joshua Slocum, Seth Norman, Elisa Novelli, Cari Anderson. Thank you for your support and feedback over the years. I wish all of you continued luck in your scientific goals.

Finally, thank you to my friends and family; your support has allowed me to achieve my goal.

Role of Local Electrostatic Fields in Protein-Protein and Protein-Solvent Interactions Determined by Vibrational Stark Effect Spectroscopy

Christina Marie Ragain, Ph.D.

The University of Texas at Austin, 2014

Supervisor: Lauren J. Webb

This examines the interplay of structure and local electrostatic fields in protein-protein and protein-solvent interactions. The partial charges of the protein amino acids and the polarization of the surrounding solvent create a complex system of electrostatic fields at protein-protein and protein-solvent interfaces. An approach incorporating vibrational Stark effect (VSE) spectroscopy, dissociation constant measurements, and molecular dynamics (MD) simulations was used to investigate the electrostatic interactions in these interfaces.

Proteins p21^{Ras} (Ras) and Rap1A (Rap) have nearly identical amino acid sequences and structures along the effector-binding region but bind with different affinities to Ral guanine nucleotide dissociation stimulator (RalGDS). A charge reversion mutation at position 31 alters the binding affinity of Ras and Rap with RalGDS from 0.1 μM and 1 μM, to 1 μM and 0.5 μM, respectively. A spectral probe was placed at various locations along the binding interface on the surface of RalGDS as it was docked with Ras and Rap single (position 30 or 31) and double mutants (both positions). By comparing the probes' absorption energies with the respective wild-type (WT) analogs, VSE spectroscopy was able to measure molecular-level electrostatic events

across the protein-protein interface. MD simulations provided a basis for deconvoluting the structural and electrostatic changes observed by the probes. The mutation at position 31 was found to be responsible for both structural and electrostatic changes compared to the WT analogs. Furthermore, previous identification of positions N27 and N29 on RalGDS as "hot spots" that help discriminate between structurally similar GTPases was supported.

The RalGDS probe-containing variants and three model compounds were placed in aqueous solvents with varying dielectric constants to measure changes in absorption energy. We investigated the ability of the Onsager solvent model to describe the solvent induced changes in absorption energy, while MD simulations were employed to determine the location and solvation of the probes at the protein-solvent interface. The solvent accessible-surface area, a measure of hydration, was determined to correlate well with the change in magnitude of the probe's absorption energy and the displaced solvent by the probe.

Table of Contents

List of Tables

List of Figures

Chapter 1: Introduction

1.1 PROTEINS AND ELECTROSTATIC FIELDS

A complex set of electrostatic fields is created by the partial charges of the amino acid residues in a protein and the polarization of the solvent at the protein-protein and protein-solvent interfaces. These electrostatic fields play a role in all protein functions including folding, chemical reactivity, and enzyme kinetics, as well as protein-solvent, protein-ligand and protein-protein interactions.[1-3] Though measurement of these electrostatic fields is difficult, they have been estimated to be heterogeneous and range over 10s of MV/cm.[4-6] Understandably, the interplay between electrostatic fields and molecular structure at protein-protein and protein-water interfaces has been a long-standing question in the biophysical community.[1-3,7-11]

1.2 MEASURING ELECTROSTATIC FIELDS

Until recently, a direct experimental method to measure electrostatic fields in proteins had not existed. The only experimental methods were indirect measurements in which the interpretation of pKa shifts[12-14] and ^{19}F NMR chemical shifts,[15,16] were used to calculate protein electrostatics. Furthermore, the development of computational methods for predicting electrostatic fields[1,2] in proteins has been of great interest in the theoretical community. A significant challenge has been the lack of a good experimental method to measure local protein electrostatic fields to test and validate computational predictions.

Vibrational Stark effect (VSE) spectroscopy is a novel biophysical technique well suited for determining local electrostatic fields in proteins.[4,6,17-21] The schematic of a general VSE spectroscopic experiment is shown in Figure 1.1. In this setup, an infrared probe is inserted into a protein system of interest at a known and controllable site. The

1
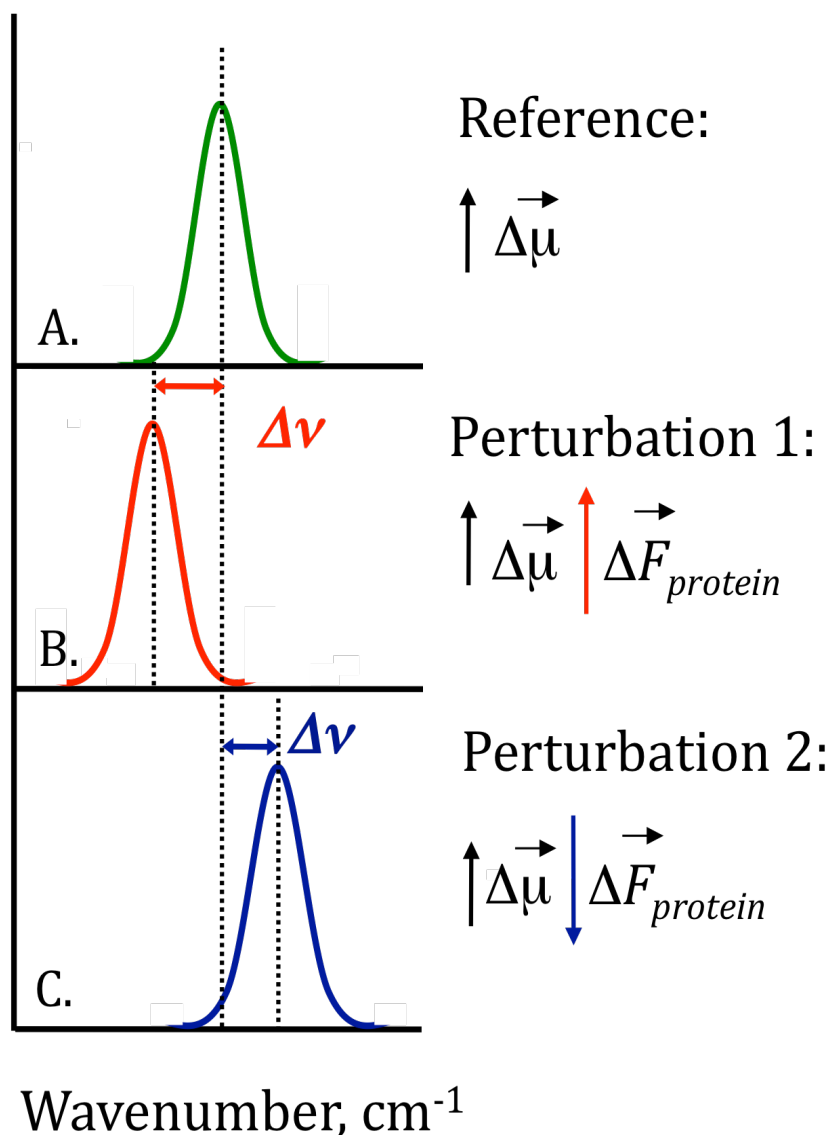
Figure 1.1. Scheme describing VSE spectroscopy strategy. A. The absorption of a VSE spectral probe is measured in a reference state. B. A perturbation to the system where $\Delta\vec{F}$ is parallel to $\Delta\vec{\mu}$ results in lowering the vibrational energy of the VSE spectral probe by $\Delta\nu$. C. A perturbation to the system where $\Delta\vec{F}$ is antiparallel to $\Delta\vec{\mu}$ results in increasing the vibrational energy of the VSE spectral probe by $\Delta\nu$.

absorption energy of the probe is recorded in a reference state (Figure 1.1A), which is carefully chosen based on the experimental question. This is due to the nature of the technique as VSE spectroscopy is a difference measurement that directly measures *changes* in the local electrostatic environment of a spectral probe. Once a perturbation is made to the system (Figure 1.1B and Figure 1.1C), the probe's vibrational absorption energy is measured again. In the work described here, the perturbation takes the form of a functional mutation that is made to the protein system (Chapters 3 and 4) or a change in the dielectric of the solvent surrounding the protein (Chapter 5). The difference in the probe's absorption energy (ΔE) relative to the reference state is calculated and then related to the change in the probe's local electrostatic field ($\Delta \vec{F}$) by an amount determined by the direction and strength of the probe's local difference dipole moment ($\Delta \vec{\mu}$), Equation 1.1. The difference dipole moment is sometimes called the Stark tuning rate and refers to the difference between the dipole moment of the probe in the ground state *versus* the first excited vibrational state.

$$\Delta E = hc\Delta v = -\Delta \vec{\mu} \bullet \Delta F \qquad (1.1)$$

Although several useful probes have been identified, the Webb group currently uses the nitrile group, a good compromise between ease of incorporation and sensitivity.[6] The nitrile is easily incorporated as a thiocyanate (SCN) through a post-translational modification of a cysteine, a procedure that will be discussed in greater detail in Chapter 2. A benefit of this probe is that the absorption energy of the nitrile stretching vibration at ~2160 cm^{-1} is outside of the complex infrared spectrum of the protein. Moreover, the SCN probe has a $\Delta \vec{\mu}$ of 0.7 MW/cm/cm^{-1},[5] which is large enough to be sensitive to the field variations estimated to be present in proteins.[4-6] The SCN probe is shown in Figure 1.2 with the direction of $\Delta \vec{\mu}$, which is parallel to the nitrile bond vector, indicated with an arrow above the structure.
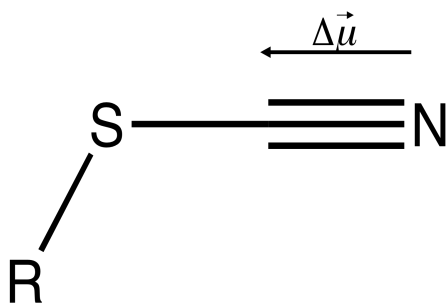
Figure 1.2. The thiocyanate probe (SCN) is shown. The difference dipole ($\Delta\vec{u}$) is parallel to the nitrile bond and its direction is indicated with an arrow above the structure.

1.3 THE PROTEIN-PROTEIN MODEL SYSTEM

Two human proteins, p21[Ras] (Ras) and Rap1A (Rap) and their downstream effector, Ral guanine nucleotide dissociation stimulator (RalGDS), were selected for use in these experiments to investigate the connection between local electrostatic fields and binding specificity at the protein-protein interface. Ras and Rap are members of the Ras superfamily of guanosine triphosphate (GTP) hydrolyzing proteins (commonly referred to as GTPases), which switch between an ON state when GTP-bound and an OFF state when guanosine diphosphate (GDP)-bound in the regulation of signaling pathways.[22] Ras and Rap are carefully regulated through interactions with other proteins during their catalytic cycle, as shown in Figure 1.3. In their ON-state, GTPases dock to the Ras-binding domain of downstream effectors to propagate cellular messages. As members of the Ras family of GTPases, Ras and Rap are poor GTPases; interactions with a GTPase activating protein (GAP) increases the hydrolysis of GTP to GDP, which switches the GTPase into its OFF-state. A G-nucleotide dissociation inhibitor (GDI) keeps the GTPase from exchanging GDP for GTP until needed and G-nucleotide exchange factors (GEF) aid the GTPase to exchange GDP for GTP, switching the protein back to the ON-state.

Ras and Rap are shown in Figure 1.4 complexed with c-Raf-1 (Raf) and RalGDS, two downstream effector proteins. As members of the Ras family, Ras and Rap are structurally similar, with 50% overall matching amino acid sequences, 80% amino acid homology, and nearly identical structural and effector binding surfaces (with a root mean squared deviation (RMSD) of 0.7 Å for homologous residues).[23] Despite their structural similarity, Ras and Rap are involved in distinct cellular processes. Ras plays a role in cell division, cell survival, and apoptosis.[24-26] Whereas, Rap is involved in cellular adhesion.[27,28] The origin of this functional specificity lies in the ability of Ras and Rap to bind to different downstream effectors while in the GTP-bound ON state, initiating
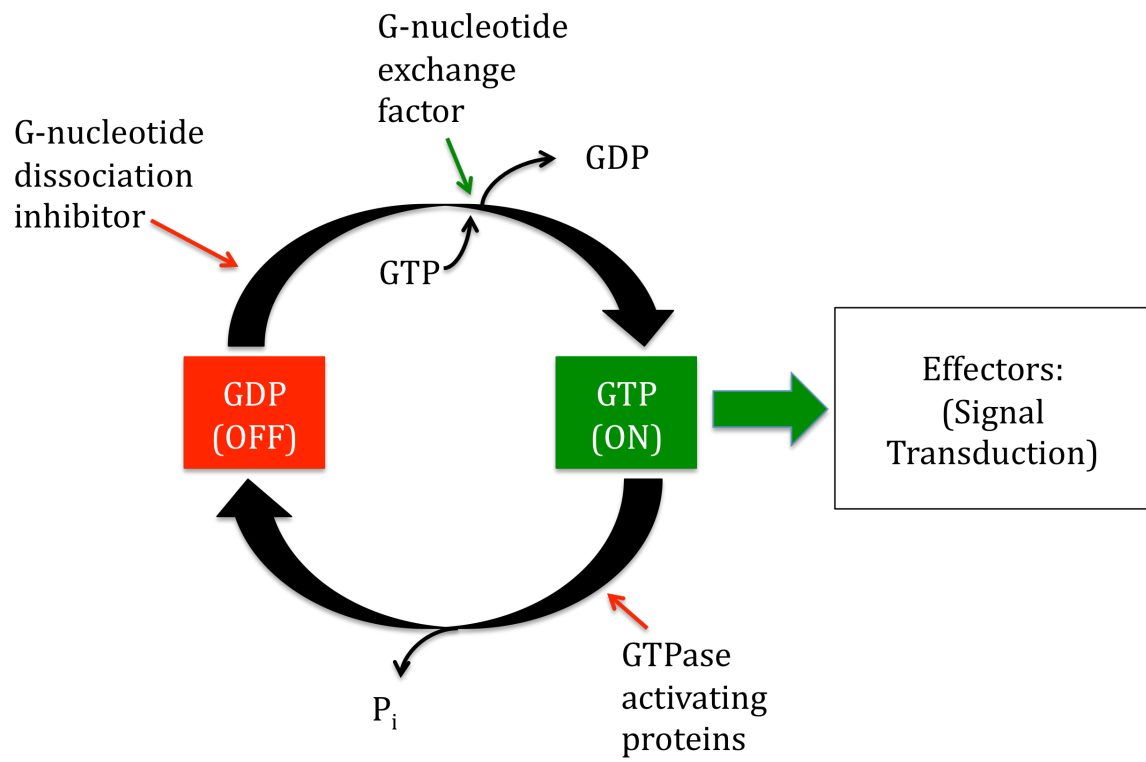
Figure 1.3.   The catalytic cycle of Ras and Rap.[22]
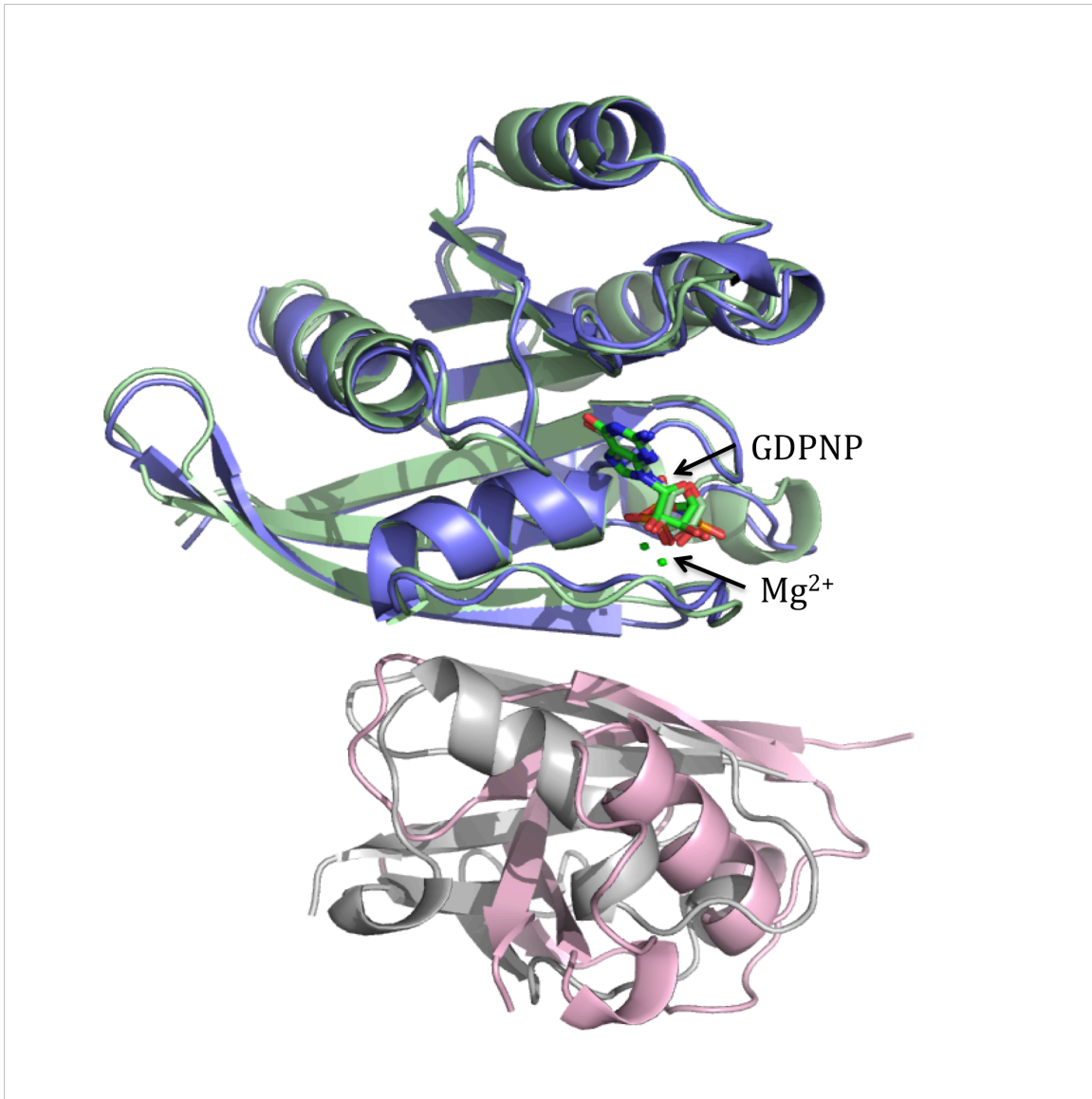
Figure 1.4. Alignment of the x-ray crystal structures of Ras (E31K, green) complexed with RalGDS (gray) from 1LFD[29] overlaid with Rap (E30D/K31E, blue) complexed with Raf (pink) from 1GUA.[23] The figure was prepared by aligning Rap to Ras.

different signaling cascades. For example, Raf is a downstream effector of Ras, binding to Ras with a dissociation constant (K_d) 100-fold lower than that of Raf to Rap.[30] Similarly, Rap binds to a second downstream effector, Ral guanosine dissociation stimulator (RalGDS), with a K_d that is 10-fold tighter to Rap than RalGDS-to-Ras.[30] The structural similarity between Ras and Rap indicates that structural factors alone cannot explain the difference in binding discrimination for the downstream effectors, making Ras and Rap an ideal model system to explore the role of protein electrostatic fields in protein-protein interactions.

In the binding region, Ras and Rap have nearly identical amino acid sequences, differing only at positions 30 and 31. Position 30 is glutamic acid (E) in Rap and aspartic acid (D) in Ras. Both residues are negatively charged and differ only by one methylene group. On the other hand, Position 31 is a positively charged lysine (K) in Rap and a negatively charged glutamic acid (E) in Ras. In 1995, Herrmann and coworkers demonstrated the importance of the amino acids at positions 30 and 31 of Ras and Rap in discriminating downstream effector partners.[23,30] The studies found that the charge reversion mutation Rap K31E and the double mutation Rap E30D/K31E resulted in an increased K_d between the Rap mutant and the downstream effector RalGDS to values similar to interactions between wild-type (WT) Ras and RalGDS.[30] Furthermore, the double mutant Rap E30D/K31E co-crystallized with the downstream effector Raf, which usually binds more strongly to Ras.[23] Similarly, the mutation Ras E31K was used to co-crystallize Ras with RalGDS (normally Rap's immediate downstream effector).[29] The single reversion mutant Ras E31K also had significantly reduced binding affinity with Raf.[31] Therefore, the charge on position 31 must provide Ras and Rap an electrostatic mechanism for binding discrimination.

Recently, VSE spectroscopy was used to compare docked complexes of RalGDS with WT Ras and WT Rap by examining the changes in absorption energy of an SCN probe at various locations on RalGDS.[6] In certain probe locations, the change in absorption upon binding to WT Ras and WT Rap was similar in both direction and magnitude. In other locations, the magnitudes of the absorption energy changes were different, suggesting that these amino acids may participate in an electrostatic mechanism that enables RalGDS to distinguish Ras from Rap. Additionally, measurement of the dissociation constant for docking the GTPases with SCN-containing Ral mutants showed no deleterious effects on the formation of the docked complex due to the presence of the spectroscopic probe. These measurements were later confirmed through extensive molecular dynamics sampling of the protein-protein complex.[32] Therefore, these RalGDS-based SCN probes are ideal for investigating the electrostatic mechanism for binding discrimination as mediated by the charge on position 31 in Ras and Rap. The use of SCN-labeled RalGDS variants in the investigation of the position 30 and 31 amino acid reversions is described with respect to Rap in Chapter 3 and Ras in Chapter 4.

1.4 THE PROTEIN-SOLVENT MODEL SYSTEM

1.4.1 RalGDS and Organic Molecules

Thiocyanate probes at nine locations on RalGDS and three small molecules – methyl thiocyanate (MeSCN), ethyl thiocyanate (EtSCN), and hexyl thiocyanate (HxSCN) – served as the model systems for the investigation of protein-solvent interactions. A recent study measured the absorption energies of a series of SCN-labeled RalGDS variants and found that the absorption energy of each probe varied based on its location, despite each probe being solvent exposed.[6] Due to the placement of the SCN probe at the protein surface, these studies are strongly influenced by both molecular and

continuum effects of the solvent. The former would cause changes in absorption energy based on hydrogen bonding, while the later would cause changes in absorption energy based on purely electrostatic effects. MD simulations were employed to attempt to disentangle these two effects, focusing on the location of the nitrile probe at the protein-solvent interface. The absorption energy of the different probe locations was found to correlate with each probe's solvent accessible surface area (SASA)[6] suggesting that different probe locations may react differently to changes in solvent. Chapter 5 describes the investigation of the changes in absorption energy of SCN probes from changes in the dielectric of the solvent at 9 locations on RalGDS and in 3 model compounds.

1.4.2 Onsager Solvation Model

A simple model, the Onsager solvation model,[33] was used to describe the solvent in the studies here. In the Onsager solvation model, placing a chromophore into a solvent creates a solvent cavity that orients and polarizes the surrounding solvent molecules, which in turn polarizes the chromophore and creates a reaction field. In these studies, the chromophore is the SCN probe on the protein surface. The reaction field, $\vec{F}_{Onsager}$, is related to the permanent dipole of the chromophore, $\vec{\mu}_0$, the polarizability of the solvent represented by the dielectric constant of the solvent, ε, and the polarizability of the chromophore represented by the refractive index of the chromophore, n, through Equation 1.2.[33]

$$\vec{F}_{Onsager} = \frac{\vec{\mu}_0}{a^3}\left[\frac{2(\varepsilon-1)(n^2+2)}{3(2\varepsilon+n^2)}\right]$$

(1.2)

In this equation, a is the radius of the spherical solvent cavity taken up by the chromophore.[33] Previous work has used the vibrational absorption energies of various benzonitriles to compare with the calculated Onsager factor (hereafter Φ), the bracketed

portion of Equation 1.2.[34] According to the Stark equation, the absorption energies, ν, of the SCN probes can be related to the reaction field according to Equation 1.1. The slope (m) of ν *versus* Φ should be linear and related to the dot product of the permanent dipole moment, μ_0, and the Stark tuning rate as shown in Equation 1.3. [34]

$$m = \frac{-\Delta\vec{\mu} \bullet \vec{\mu}_0}{hca^3} \tag{1.3}$$

Recently, Levinson and coworkers reported the successful use of Stark effect theory with the Onsager solvation model to describe the solvatochromic shifts of nitrile probes on substituted benzonitriles in a series of aprotic solvents of varying dielectric constants.[34] These results were remarkable in that the simple continuum Onsager model, which does not take molecular details of the solute or solvent into account, was able to reproduce the vibrational solvatochromism of a series of small-molecule nitrile probes.[34] The experimental model system used in the Levinson study was ideal in that there was no convoluting factor of hydrogen bonding between the solvent and the nitrile potentially disrupting the clear correlation between electrostatic environment and vibrational absorption energy. We were interested in determining whether these results could also describe the solvatochromism of a nitrile probe in a significantly more complex environment: at the interface between a protein and a protic solvent. In this environment, the probe is not surrounded by a uniform cavity of radius a and could potentially be hydrogen bonded to the solvent. The extent to which a simple Onsager model describes the relationship between the measured absorption energy and local reaction field is compared to local chemical and structural factors in the immediate environment of the probe to catalog cases when VSE appeared to be convoluted with important structural parameters such as hydrogen bonding.

Chapter 2. Materials and Methods

2.1. PROTEIN EXPRESSION AND PURIFICATION

2.1.1 WT RalGDS and Mutants

The construct for the wild-type (WT) Ral guanine nucleotide dissociation stimulator (RalGDS) was composed of residues 790-866, which make up the 97-residue, Ras-binding domain of RalGDS and an N-terminal hexa-histadine (hexa-His) tag with a thrombin cleavage site. The construct was synthesized and cloned into the pET-15b expression vector (Novagen) by GenScript (Piscataway, NJ) and the sequence was confirmed through DNA sequencing. For clarity, we adopt the numbering convention of the RalGDS crystal structure, 1LFD, which indexes the glycine at position 797 in RalGDS as G14.[29] The incorporation of the vibrational Stark effect (VSE) spectral probe requires a post-translational modification to an exposed cysteine. Previously, the WT cysteines, C16 and C17, were mutated to alanine to avoid the introduction of a secondary probe; the cysteine-less complex will be referred to as Ralβ.[6] Nine constructs for Ralβ mutants with a mutation to add a cysteine at selected amino acid locations, I18C, R20C, N27, G28, N29, Y31, K32, S33C and N54, were obtained from a previous study.[6]

Expression and purification of Ralβ mutants followed previously established protocols.[6] Two liters of sterile terrific broth (TB) media with 100 mg/L ampillicin were inoculated with the BL21(DE3) strain of *Escherichia coli* (*E. coli*) containing the RalGDS variant plasmid and agitated at 37 °C until the optical density at 600 nm (OD_{600}) reached 0.6, the linear growth phase of the *E. coli*. Upon the addition of 1 mM isopropyl *β*-D-1-thiogalactopyranoside (IPTG), protein expression was triggered. Finally, the

temperature was decreased to 18 °C and the cultures were agitated for 16-20 hrs overnight.

Cells were collected by centrifugation, resuspended in lysis buffer (50 mM sodium phosphate, 500 mM NaCl, 20 mM imidazole, pH = 8.0) and lysed by sonication. Cell debris was removed by centrifugation and the clarified lysate was passed through a 10 μM filter. For the first step of purification, lysate containing the hexa-His tagged RalGDS was loaded onto a 5 mL HisTrapFF (GE Healthcare) column at a flow rate of 2 mL/min; the amount of protein flowing off the column was monitored by absorption at 280 nm. The column was washed with 5 column volumes of lysis buffer or until the absorption at 280 nm returned to baseline. The hexa-His tagged RalGDS was eluted from the column using a gradient of 0-100% His elution buffer (50 mM sodium phosphate, 500 mM NaCl, 500 mM imidazole, pH = 8.0) over 30 minutes. The fractions containing hexa-His tagged RalGDS were pooled. The hexa-His tagged RalGDS was exchanged in the thrombin cleavage buffer (20 mM Tris, 150 mM NaCl, 2.5 mM CaCl$_2$, pH = 8.0). The concentration of hexa-His tagged RalGDS was estimated using its absorption at 280 nm (ε=7,450 M^{-1}cm^{-1}). The hexa-His tag was cleaved by the addition of 1 unit (U) of thrombin per 1 mg Ral and incubating the mixture overnight at 4 °C. Cleaved RalGDS was exchanged into ion-exchange loading buffer (50 mM Tris, pH = 8.0) and loaded onto a 5 mL HiTrap Q HP column (GE Healthcare) at 2 mL/min. The column was washed with 5 column volumes of ion-exchange loading buffer or until the absorption at 280 nm returned to baseline. RalGDS was eluted from the column using a 0-100% gradient of ion-exchange elution buffer (50 mM Tris, 1 M NaCl, pH = 8.0). The fractions containing the RalGDS variant were pooled and transferred into labeling buffer (50 mM Tris pH = 7.5, 100 mM NaCl). Aliquots were flash frozen and stored at -80 °C for further experiments.

13

2.1.2 His-Tev

The hexa-His-tagged tobacco etch virus protease (His-TEV) construct with the mutation S219V was obtained from Addgene (Addgene plasmid 8827).[35] Expression and purification of His-Tev followed previously established protocols.[6,35] One liter of sterile TB media with 100 mg/L ampillicin and 30 mg/L chloramphenicol was inoculated with the BL21(DE3) strain of *E. coli* containing the His-Tev plasmid and agitated at 37°C until the OD_{600} reached 0.6. Expression was triggered by the addition of 1 mM of IPTG and the culture was agitated for 4 h at 30 °C. Cells were collected by centrifugation and resuspended into lysis buffer. The resuspended cells were lysed by sonication and 0.1 % polyethylenamine was added to precipitate nucleic acids. Cell debris was removed by centrifugation.

The clarified lysate was passed through a 10 μM filter and loaded onto a 5 mL His-Trap FF column (GE Healthcare) at 2 mL/min. The column was washed with lysis buffer until the absorption at 280 nm returned to the baseline. His-Tev was eluted with a 0-100% gradient of His-elution buffer. Fractions containing His-Tev were pooled and concentrated to 3 mL. 1 mM of ethylenediaminetetraacedic acid (EDTA) and dithiothreitol (DTT) was added to the protein solution and the solution was loaded onto an S-100 gel filtration column (GE Healthcare) previously equilibrated in 25 mM sodium phosphate, pH = 8, 200 mM NaCl, 10% glycerol, 2 mM EDTA, 10 mM DTT. The protein was eluted in 140 mL; this aliquot was flash frozen and stored at -80 °C.

2.1.3 WT Ras and Mutants

The gene construct for the human H-Ras (Ras), composed of residues 1 – 166, on the pProEX vector (Invitrogen), was obtained from a previous experiment.[6] The construct also contained a hexa-His N-terminal tag with a tobacco etch virus protease (TEV) cleavage site. To investigate the roles of positions 30 and 31 in the binding specify of

downstream effector proteins for Ras *versus* Rap, three Rap-like reversion mutants (D30E, E31K, and D30E/E31K) were constructed using the Quikchange mutagenesis kit (Stratagene) with polymerase chain reaction (PCR) primers obtained from Sigma-Aldrich. Expression and purification of WT and mutant Ras followed the protocols established for WT Ras as previously reported.[6] Two liters of sterile TB media with 100 mg/L ampillicin were inoculated with the BL21(DE3) *E. coli* containing the Ras variant plasmid and Ras was expressed following the protocols described above for RalGDS. Following expression, the cells were collected by centrifugation and lysed by sonication. Cell debris was removed from the lysate by centrifugation.

The clarified lysate was passed through a 10 mM filter and loaded onto a HisTrapFF (GE Healthcare) column as described for RalGDS. The purified Ras was transferred into TEV cleavage buffer (50 mM Tris, 50 mM NaCl, pH = 8.0). The concentration of the hexa-His tagged Ras was estimated by absorbance at 280 nm (ε=11,200 M^{-1} cm^{-1}) and 10 mg of His-TEV was added per 100 mg of purified Ras to cleave the hexa-His tag. The His-TEV/Ras solution was incubated overnight at 4 °C. The protein solution was spiked with 20 mM of imidazole and 300 mM of KCl and loaded onto a second HisTrapFF (GE Healthcare) column at 2 mL/min. Without the hexa-His tag, Ras flowed through the column. Cleaved Ras was collected in the flow through and the first column volum of a wash with lysis buffer. The Ras variant was concentrated using a centrifugation filter (Millipore) to 2-3 mL, transferred into labeling buffer, flash frozen and stored at -80°C for further experiments.

2.1.4 WT Rap and Mutants

The WT Rap construct was composed of residues 1-167 of Rap 1A and contained an N-terminal hexa-His tag with a thrombin cleavage site. The WT Rap gene construct

was synthesized and cloned into the pET-15b expression vector (Novagen) by GenScript (Piscataway, NJ) and the sequence confirmed. To investigate the role of the amino acid identity at positions 30 and 31, three Ras-like reversion mutants (Rap E30D, Rap K31E, and Rap E30D/K31E) were made to Rap using the Quikchange mutagenesis kit (Stratagene) with PCR primers obtained from Sigma-Aldrich. WT and mutant Rap vectors (Rap E30D, Rap K31E, and the double mutant Rap E30D/K31E) were transformed into the *E. coli* strain Arctic Express (DE) (Stratagene), and expression and purification were carried out as previously reported.[6] Two liters of sterile TB media with no antibiotics were inoculated with *E. coli* containing the Rap variant plasmid and agitated at 37 °C until the OD_{600} reached 0.6. The temperature was reduced 11 °C and selection antibiotics (100 mg/L ampicillin and 30 mg/L gentamycin) were added. Protein expression was induced by the addition of 1 mM IPTG and 1 mM DTT. The cultures were then agitated for 24 hrs. Cells were collected by centrifugation and resuspended in lysis buffer containing 10% glycerol and 1 mM DTT. The Rap variants were purified following the procedure described for the RalGDS. Following purification, the Rap variant was exchanged into loading buffer, flash frozen and stored at -80 °C for further experiments.

2.2 LOADING WITH NUCLEOTIDE

Ras and Rap interact with their downstream effectors in their GTP-bound (ON-state). To ensure that the Ras and Rap variants were in their ON-state during the kinetics and spectroscopic studies, they were loaded with a GTP analog. The nonhydrolyzable GTP analog, GDPNP (guanosine 5'-[β,γ-imido]triphosphate trisodium salt hydrate, Sigma), was used for spectral experiments. Whereas, the fluorescently labeled GTP, mant-GTP (2′-(or 3′)-O-(N-methylanthraniloyl)guanosine 5′-triphosphate trisodium salt,

Invitrogen), was used for the determination of dissociation binding constants.[6] The concentration of the protein was determined by the absorption at 280 nm. EDTA and DTT were added to concentrations of 4 mM and 5 mM, respectively. Additionally, either 3 times molar excess of GDPNP or 1.2 times molar excess of Mant-GTP was added to the protein solution. The solution was incubated at 4 °C for 1.5 hrs. $MgCl_2$ was added to a concentration of 10 mM. Then, the solution was incubated for an additional 30 minutes at 4 °C. Solutions containing the fluorescent GTP analog, mant-GPT, were kept covered with aluminum foil to prevent exposure to light at all times. The nucleotide-loaded GTPase was transferred to loading buffer, flash frozen and stored at -80°C for further experiments. The nucleotide-loaded protein concentration was estimated to be 80% of the concentration measured at the beginning of the loading process.

2.3 VIBRATIONAL STARK EFFECT (VSE) SPECTROSCOPY

2.3.1 Introduction of the spectral probe

The conversion of a cysteine thiol into the cyanocysteine containing the SCN probe is shown in Figure 2.1 and has been described previously.[5,6] Three molar equivalents of 5,5′- dithiobis(2-nitrobenzoic acid) (DTNB, Sigma-Aldrich) were added to a protein mutant containing one solvent-exposed cysteine residue and incubated at room temperature for 2-14 hrs, forming the protein-bound thionitrobenzoic acid disulfide (PSTNB). The formation of the thionitrobenzoic acid (TNB), a side product of the labeling reaction, was observed at 412 nm (ε=13,600 M^{-1} cm^{-1}) and used to monitor the extent of the labeling reaction. After 1 equivalent of TNB had been generated, 30 equivalents of potassium cyanide (KCN) were added to displace the protein-bound TNB and generate the protein-thiocyanate complex (PSCN). The extent of reaction was again

17
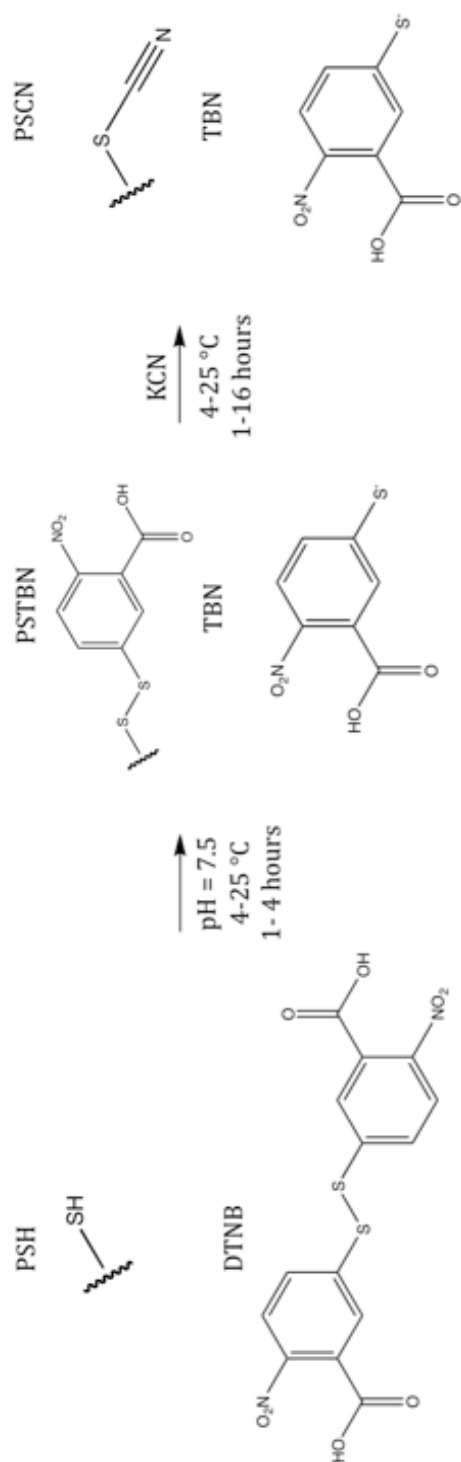
Figure 2.1. The introduction of the thiocyanate (SCN) VSE spectral probe by post-translational modification of a cysteine containing protein (PSH).[5,6]

observed by absorption of the TNB side product at 412 nm. At the end of the reaction, a PD-10 desalting column (GE Healthcare) was used to remove excess TNB and KCN and return the labeled protein to the labeling buffer. Concentrations were estimated by absorption at 280 nm (ε=7,450 M^{-1} cm^{-1}). The SCN-labeled Ralβ mutants were flash frozen and stored at -80 °C for future experiments. The SCN-labeled Ralβ mutants are denoted with the subscript "SCN."

2.3.2 Bound Complex Preparation

For the protein-protein interaction studies described in Chapters 3 and 4, complexes of the SCN-labeled Ralβ mutants bound to the GTPases variants of interest were prepared. The bound complexes were formed by the incubation of the SCN-labeled Ralβ mutants with 1.2 molar equivalents of the desired GTPase in labeling buffer at 4 °C for 2 hrs. The solution was then concentrated by centrifugation to ~2 mM. Data for the SCN-labeled Ralβ mutants bound to WT Ras and WT Rap were taken from an earlier study.[6]

2.3.3 Monomer Sample Preparation

For the protein-solvent study described in Chapter 5, the SCN-labeled Ralβ were exchanged into labeling buffer with varying concentrations of glycerol (10%, 20%, 30% or 40%) with dielectric constants of 80.37, 77.55, 74.72, 71.77 and 68.76, respectively.[36] Protein monomer solutions were concentrated by centrifugation to ~2-4 mM. Data for the monomers in labeling buffer with 0% glycerol was taken from an earlier study.[6]

2.3.4 Model Compound Preparation

Three model organic compounds were used in the protein-solvent study described in Chapter 5. Solutions of 1 mM methyl thiocyanate (MeSCN), ethyl thiocyanate

(EtSCN) and hexyl thiocyanate (HxSCN) were prepared in labeling buffer with varying glycerol concentrations (0%, 10%, 20%, 30% or 40%).

2.3.5 Fourier Transform Infrared Spectroscopy (FTIR)

Vibrational absorption spectra of the monomeric or bound complexes were collected at room temperature in a sample cell composed of 2 sapphire windows separated by 125 μm thick polyethylene terephthalate (PETE) spacers in a Bruker Vertex 70 Fourier transform infrared (FTIR) spectrometer. The sample cell was illuminated with light in the range of 2000-2500 cm^{-1} selected by a broad bandpass filter (Spectrogon, Parsippany, NJ) placed in front of the instrument's infrared source. Spectra were composed of 250 scans collected with a liquid nitrogen-cooled indium antimonide (InSb) detector at 0.5 cm^{-1} resolution. Thiocyanate absorption occurs in the same region of a large absorbance from liquid water in the buffer; therefore, background-subtracted spectra were fit with an in-house program. The absorption energy ν_{obs} and the full width at the half maximum (fwhm) were determined. This fitting strategy is shown in Figure 2.2 for a representative absorption spectrum, where a set of raw data (crosses, 2.2A) was fit to the sum of a fourth-order polynomial baseline (dashed line, 2.2A) and a normal function (dashed line, 2.2B) using a maximum likelihood fitting strategy (solid line, 2.2A). The reported spectrum (crosses, 2.2A) is obtained by taking the difference between the raw data and the fitted polynomial baseline. The residual (dotted line, 2.2B) was the difference between the fitted spectrum and the raw data, equivalent to the difference between the reported spectrum and the fitted normal function. Uncertainty in absorption energy is reported as the standard deviation of at least four measurements.
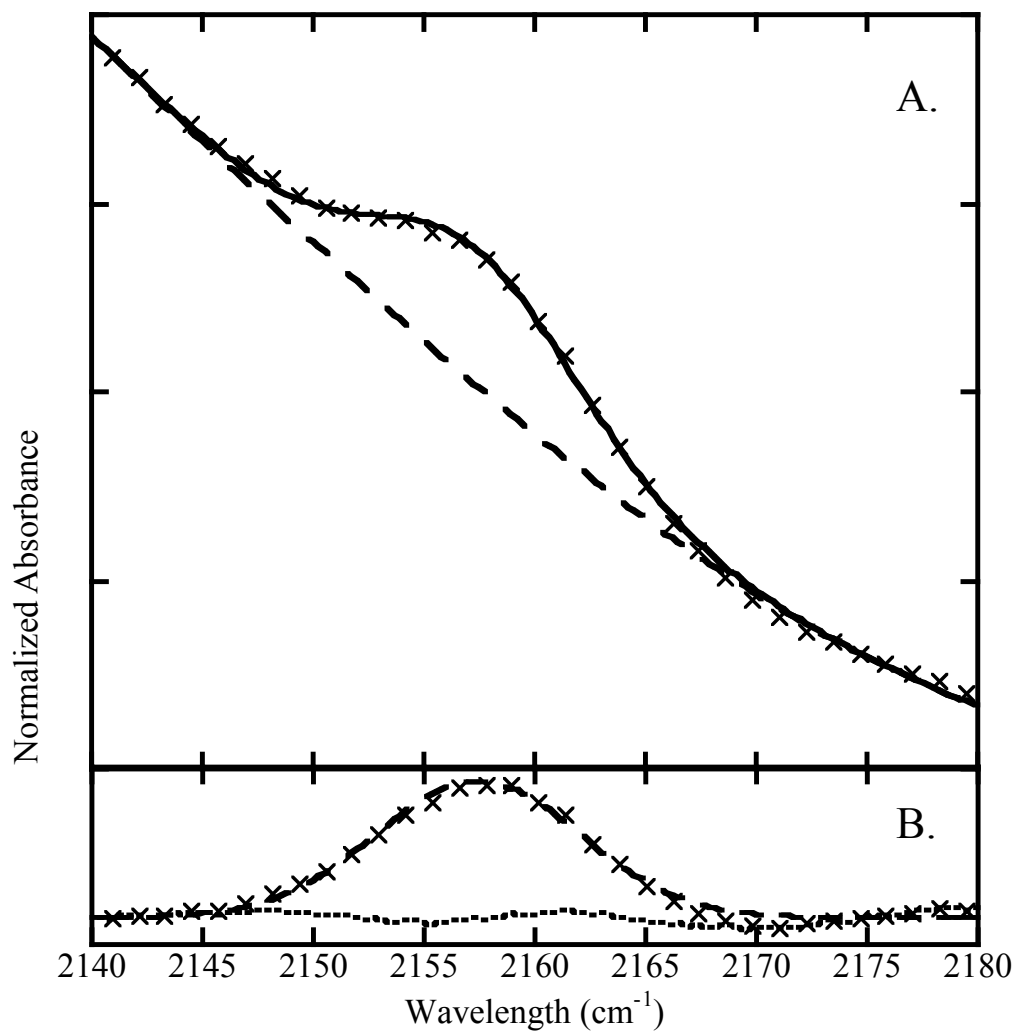
Figure 2.2. Representative example of fitting absorption spectra. A. Crosses: raw data; dashed line: baseline determined from a fourth-order polynomial; solid line: fitted spectrum, which is the sum of the fitted polynomial and fitted normal function. B. Results of the fit in A. Crosses: reported spectra, determined from the raw data from A less the baseline from A; dashed line: fitted normal function; dotted line: residuals.

2.4 DISSOCIATION CONSTANT MEASUREMENTS

Dissociation constant measurements were conducted to ensure that the addition of the SCN probe did not disrupt the binding of the SCN-labeled Ralβ probes with the Ras and Rap variants used in the spectral experiments. The dissociation constant, K_d, of the complex formation was determined using a guanine nucleotide dissociation inhibition (GDI) assay described previously.[6,17,37] The GTPase (Ras or Rap variant) containing mant-GTP was incubated with varying concentrations of the Ras-binding domain of interest (WT RalGDS or a SCN-labeled Ralβ mutant) at 4°C for 1-2 hrs in a 96-well top reading fluorescence plate (Sigma). The dissociation of mant-GTP was initiated by the addition of 2.5 mM GDPNP. The SpectraMax M3 multi-mode microplate reader (Molecular Devices) mixed the samples for 5 seconds and monitored the decay in the fluorescence of mant-GTP in real time with excitation and emission wavelengths set to 365 and 450 nm, respectively. The initial rate of this decay was taken to be the observed rate of the dissociation reaction, k_{obs}, and was fit to Equation 2.2 to determine K_d:

$$k_{obs} = k_{-1} - k_{-1} \frac{R_0 + E_0 + K_d - \sqrt{\left(R_0 + E_0 + K_d\right)^2 - 4R_0E_0}}{2R_0}$$

$$(2.2)$$

where k_{-1} is the rate constants in absence of the RBD, R_0 is the concentration of the GTPase, and E_0 is the concentration of the Ras-binding domain .[37]

2.5 MOLECULAR DYNAMIC (MD) SIMULATIONS

Interpretation of the FTIR spectral data in vibrational Stark effect spectroscopy requires knowledge of the orientation of the probe oscillator. Molecular dynamics simulations were carried out by Mr. Andrew Ritchie, also in the Webb group, to determine probable orientations of each Ralβ-based SCN probe and the 30 and 31 side chains of the GTPase of interest.

2.5.1 Rap-Ral System

For the Rap-Ral complexes, Mr. Ritchie started from the Rap crystal structure 1GUA[23] and modeled in the N-terminal GSH tag.[17] The starting structures for the six SCN-labeled Ralβ mutants used for these simulations were obtained previously.[6] To create the Rap/Ral complexes, WT Rap was aligned by the molecular visualization system, PyMol,[38] to starting structures of the previously used structures for the Ras E31K complexes with SCN-labeled Ralβ mutants.[6] Rap residues at positions 30 and 31 for each of the docked mutant complex were mutated using AmberTools.[39] The Rap-Ral complexes were solvated in a tip3p[40] water box. Umbrella sampling in GROMACS[41] was used to extensively sample the χ_2 dihedral angle, Cα-Cβ-Sγ-Cδ, of the SCN-probe and the χ_1 dihedral angle, N-Cα-Cβ-Cγ, of the Rap 30 and 31 side chains. Full experimental details for the MD simulation are reported in Reference 17.

2.5.2 Ras-Ral system

For the Ras-Ral complexes, Mr. Ritchie used SCN-labeled Ralβ mutants structures and WT Ras that were obtained previously.[6] Ras residues at positions 30 and 31 for each docked mutant complexes were mutated using AmberTools.[39] The Ras-Ral complexes were solvated in a tip3p[40] water box. Umbrella sampling in GROMACS[41] was used to extensively sample the χ_1 and χ_2 dihedral angles, N-Cα-Cβ-Sγ and Cα-Cβ-Sγ-Cδ, of the SCN-probe and the χ_1 dihedral angle, N-Cα-Cβ-Cγ, of the Rap 30 and 31 side chains. Full experimental details for the MD simulation are reported in Reference 38.

2.5.3 Ral monomer system

Mr. Richie used previously obtained starting structures for the SCN-labeled Ralβ mutants.[6] The SCN-labeled Ralβ mutants were solvated in a tip3p[40] water box. Two dimensional umbrella sampling in GROMACS[41] was used to extensively sample the χ_1

and χ_2 dihedral angles, N-Cα-Cβ-Sγ and Cα-Cβ-Sγ-Cδ, of the SCN-probe. Full experimental details for the MD simulation are reported in Reference 39.

2.5.4 MD Analysis

Mr. Ritchie used the weighted-histogram analysis method (WHAM)[42,43] to deconvolute the simulated torsional distributions to determine a Boltzmann-weighted ensemble of structures for each system studied. All simulations were analyzed for convergence by examining the weighted-histogram analysis method (WHAM)-derived torsional distributions for the first half and the last half of simulation. For the Rap-Ral and Ras-Ral complexes, he defined two angles to analyze the three-dimensional probe orientations in space, the azimuthal angle (θ) and the polar angle (ϕ), which were defined using the Rap (or Ras)-Ral interfacial plane or the polar axis, respectively. For the Ral monomer system, an elevation angle was defined for the SCN-probe in respect to the protein-water surface. Full experimental details for these analyses are reported in References 17, 38 and 39.

Chapter 3. The Role of Electrostatics in Differential Binding of RalGDS to Rap Mutations E30D and K31E Investigated by Vibrational Spectroscopy of Thiocyanate Probes

In this chapter, we describe the systematic investigation of the effect of the E30D and K31E mutations to Rap on the local electrostatic fields in the downstream effector-GTPase complex measured using vibrational Stark effect (VSE) spectroscopy, molecular dynamics (MD) simulations, and dissociation constant (K_d) measurements.[17] For incorporation of the thiocyanate (SCN) VSE spectral probe, we selected six amino acids on Ral that are positioned in the protein-protein interface near positions 30 and 31 of Ras and Rap when the docked complex is formed: N27, G28, N29, Y31, K32, and N54. The locations of these amino acids within the Rap-Ral interface, as well as Rap positions 30 and 31, are shown in Figure 3.1. Positions N27 and Y31 were selected because at these probe locations we previously measured a significant difference in the absorption energies of the probes between docking of WT Ras *versus* WT Rap1A and we wanted to investigate whether these observations were due to the different amino acid identity at positions 30 and 31. Position N29 was chosen because, along with position N27, molecular dynamics (MD) structural sampling of the thiocyanate side chain within the docked complex showed that the nitrile group has the largest angle with respect to the Ras-Ral interfacial plane of the collection of Ral-based probes we have investigated, approximately 45° from the plane of the Ras-Ral interface.[6] Because the effect of the change in electrostatic field is due to the portion of the field that projects onto the nitrile probe bond axis, these positions seemed likely to respond to changes in the field vector at positions 30 and 31 of Rap, which appear from the crystal structures 1LFD[29] and 1GUA[23]
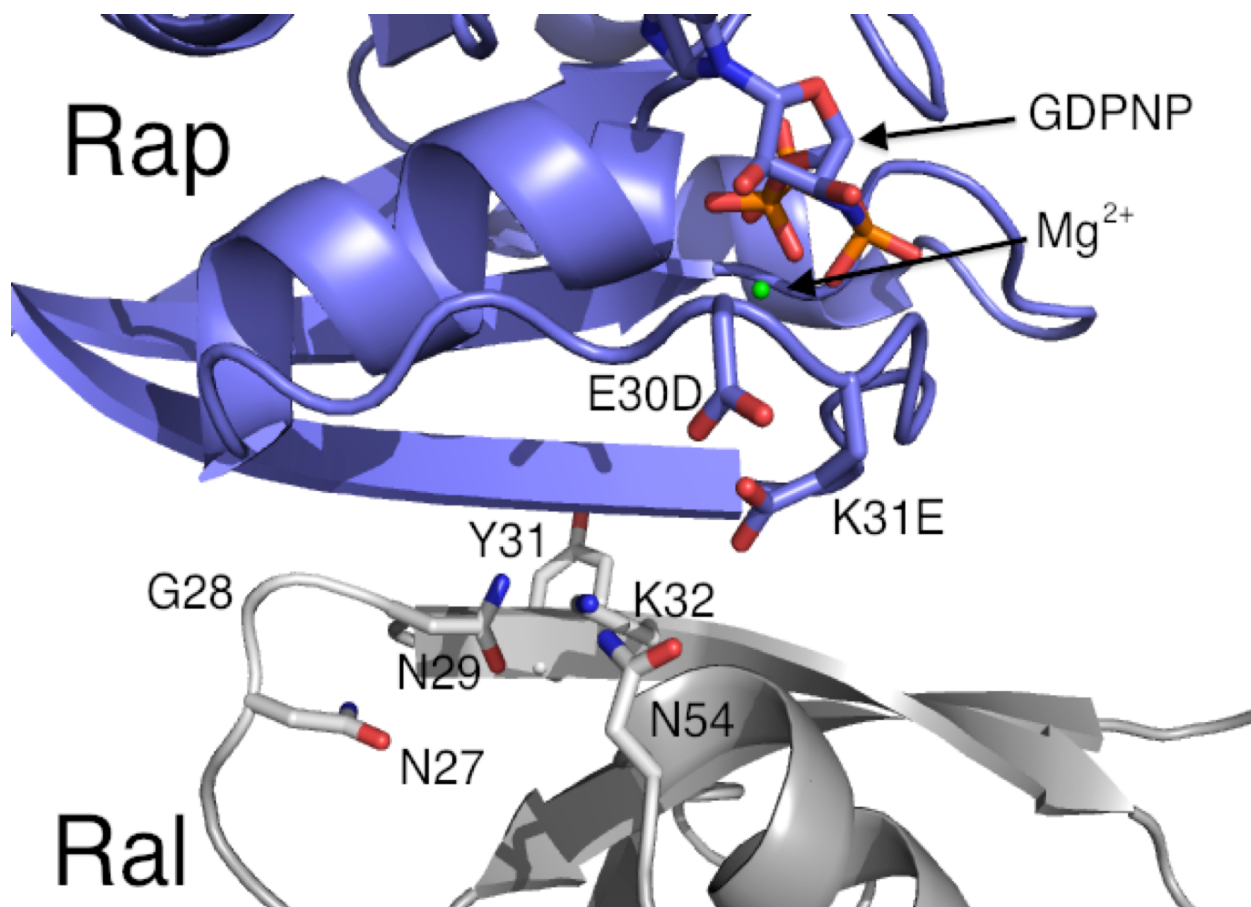
Figure 3.1. The Rap (blue)-Ral (gray) interface, highlighting Rap E30D and K31E and six amino acids on Ral that were selected for positioning the thiocyanate VSE probe in this study. The figure was prepared by aligning Rap from 1GUA[23] (containing the mutations E30D/K31E) to Ras docked with Ral from 1LFD.[29]

to be approximately perpendicular to the interface. Gly28 was chosen as intermediate between these two residues. Finally, positions K32 and N54 were selected based on their physical proximity to the side chains of positions 30 and 31 on the GTPase once the docked complex formed.

Each of the six Ral amino acids was mutated to a cysteine group, and then chemically modified to introduce the nitrile VSE probe in the form of a thiocyanate group. These mutants were then bound to WT Rap, Rap E30D, Rap K31E, and the double mutant Rap E30D/K31E. The dissociation constant, K_d, of the docked complex was determined through a fluorescence assay and the incorporation of the SCN probe was determined not to disrupt the binding interface. Extensive MD simulations on docked complexes of all Rap and Ral variants were conducted by Mr. Andrew Ritchie to determine Boltzmann-weighted orientational data for the Ral-based nitrile probes and for the side chains at Rap positions 30 and 31. These simulations demonstrate that the K31E mutation is almost exclusively responsible for changes in side-chain orientations at Rap positions 30 and 31 that cause the observed change in K_d. Finally, the difference in vibrational absorption energy, $\Delta\nu_{obs}$, of the SCN probe between the Ral/WT Rap and Ral/mutant complex was measured by Fourier transform infrared spectroscopy (FTIR). VSE spectroscopy demonstrates that only two of the probe locations examined, N27C and N29C, displayed a change in the absorption energy upon binding the Ras-like Rap double mutants that strongly resembled WT Ras. However, several of these probes did respond in an additive manner to the individual single mutations. These studies support both a structural and electrostatic mechanism to explain the observed differences in GTPase-effector binding.

27

3.1 DISSOCIATION CONSTANT MEASUREMENTS

Any effect of the thiocyanate probe on the formation of the interface can be investigated by comparing K_d values obtained for WT Ral *versus* the SCN-labeled Ralβ mutants docking to WT Ras and WT Rap; these are reported in Table 3.1. The dissociation constants presented in Table 3.1 demonstrate that the presence of the SCN probe on Ralβ mutants did not substantially affect binding to either WT Ras or WT Rap, as has been observed before.[6] The two largest deviations, caused by Ralβ G28C$_{SCN}$ (reduced K_d by an order of magnitude) and Ralβ Y31C$_{SCN}$ (increased K_d by an order of magnitude), still showed an order of magnitude increase in K_d when binding to WT Ras as opposed to WT Rap, as is expected from our previous work. Along with results from molecular dynamics sampling of this system, described below, this is strong circumstantial evidence that the nitrile VSE probe does not significantly alter the interface formed between Rap and the SCN-labeled Ralβ mutants compared to the WT interaction. Our experimental mutagenesis and chemical labeling strategy therefore does not destroy the protein-protein interaction that we are attempting to measure.

Table 3.1 also shows that binding of WT Ral to WT Rap was approximately 10-fold faster than binding to WT Ras, as has been reported before.[6,30,37] These results confirm previous reports that the reversion mutation at Rap position 31 alters the binding interaction between Rap and Ral to resemble that of Ras and Ral. All SCN-labeled Ralβ mutants interacted with Rap K31E with a K_d 10-fold higher than with WT Rap, and this effect was preserved in the double mutant Rap E30D/K31E. The single mutation Rap E30D had no effect on binding, and all K_d values measured with that construct were essentially identical to WT Rap. It is therefore clear that the amino acid located at position 31 of the GTPase is critical in the mechanism that enables Ral to distinguish

Table 3.1. Dissociation constant, K_d, of the formation of docked complexes of WT and SCN-labeled Ralβ mutants with WT Rap, WT Ras, Rap E30D, Rap K31E and Rap E30D/K31E. All values are reported in μM and errors represent one standard deviation from multiple experiments.

GTPase	Ralβ Mutation						
	WT	N27C$_{SCN}$	G28C$_{SCN}$	N29C$_{SCN}$	Y31C$_{SCN}$	K32C$_{SCN}$	N54C$_{SCN}$
WT Rap	0.26 ± 0.09	0.30 ± 0.05	0.04 ± 0.004	0.15 ± 0.08	1.0 ± 0.1	0.69 ± 0.18	0.91 ± 0.20
WT Ras	1.4 ± 0.2	7.3 ± 2.2	4.8 ± 1.1	3.1 ± 0.6	12.9 ± 4.8	6.0 ± 2.3	4.7 ± 0.4
Rap E30D	0.24 ± 0.06	0.12 ± 0.01	0.03 ± 0.015	0.10 ± 0.02	0.89 ± 0.35	0.34 ± 0.09	0.79 ± 0.10
Rap K31E	1.8 ± 0.7	2.9 ± 0.7	8.1 ± 1.5	6.0 ± 1.1	6.2 ± 2.0	1.9 ± 0.8	2.2 ± 1.5
Rap E30D/K31E	1.0 ± 0.1	5.4 ± 1.0	2.5 ± 0.3	5.0 ± 1.7	2.0 ± 0.2	1.8 ± 0.5	1.1 ± 0.3

structurally similar but functionally distinct GTPases for appropriate binding. Exploring the structural and electrostatic components of that mechanism is the subject of the MD sampling and VSE spectroscopy discussed here.

3.2 MOLECULAR DYNAMICS SIMULATIONS

Mr. Andrew Ritchie performed umbrella sampling in GROMACS[41] about the χ_2 angle of the SCN probe and the χ_1 angle of the Rap 30 and 31 side chains for each SCN-labeled Ralβ mutant docked with WT Rap and the Rap mutants E30D, K31E, and E30D/K31E. The dihedral torsional angels were analyzed using a weighted-histogram analysis method (WHAM) to accumulate a Boltzmann-weighted ensemble of simulated orientations of the thiocyanate group and the side chains at Rap positions 30 and 31. All simulations were analyzed for convergence by examining the weighted-histogram analysis method (WHAM)-derived torsional distributions for the first half and the last half of simulation. He examined an ensemble of structures obtained from stochastic dynamic sampling and accumulated a range of possible structures that could be induced by atomic-level changes in all experimental mutants while limiting errors in probable structures due to choices made about the system, such as starting structure orientations. The end result is a set of docked snapshots that represent an ensemble of structures that could be present during our room temperature steady-state experiment, rather than a small number of crystal structures that are not likely to exist in significant populations.

To analyze our molecular dynamics simulations of the torsional distribution of the thiocyanate residue on each Ralβ mutant and of the amino acids at Rap positions 30 and 31, Mr. Ritchie defined two angles for each side chain with respect to the Rap-Ralβ surface, which we term azimuthal (θ) and polar (ϕ) angles. These two angles are shown

schematically in Figure 3.2. Figure 3.2A defines a surface plane at the interface of Rap (above the plane) and Ral (below the plane); azimuthal angles are reported relative to this plane. When the cross hairs on Figure 3.2B are translated to the Cα atom of each simulated residue on Rap or Ralβ (represented as spheres), they become the origin of the polar angles shown in Figures 3.3 and 3.4. The average azimuthal and polar angles of the nitrile probe relative to the Rap-Ralβ binding interface are shown in Figure 3.3.

As seen in Figure 3.3, mutations to positions 30 and 31 of Rap did not substantially alter the orientation of the nitrile probe at the interface. The consistency of the probe orientation in these Boltzmann-weighted ensembles is further evidence that this protein-protein interface is suitable for systematic measurements with the nitrile vibrational probe without compromising the structural integrity of the interface. Similarly, Figure 3.4A and 3.4B shows that Rap side chain 30 had little difference from either the Rap mutant or the SCN-labeled Ralβ mutant to which it was docked. In all cases, the aspartate (for E30D and E30D/K31E) or glutamate (for WT and Rap K31E) pointed approximately parallel and slightly below the Rap-Ral surface plane. This suggests that both of the aspartate and glutamate side chains at this position undergo limited motions that are not influenced by the chemical identity of position 31 or the location of the thiocyanate probe.

The side chains at Rap position 31 behaved very differently. Rap position 31 side chains were pointed significantly further below the Rap-Ralβ mutant plane (Figure 3.4C) than at position 30 (55-60° below the Rap-Ral interfacial plane, pointing back towards Ral). Unlike position azimuthal and polar angles of position 30, for which all Rap mutants behaved identically, WT Rap and Rap E30D behaved identically, while the Rap mutants K31E and E30D/K31E behaved identically (Figures 3.4C and 3.4D). Taken

31
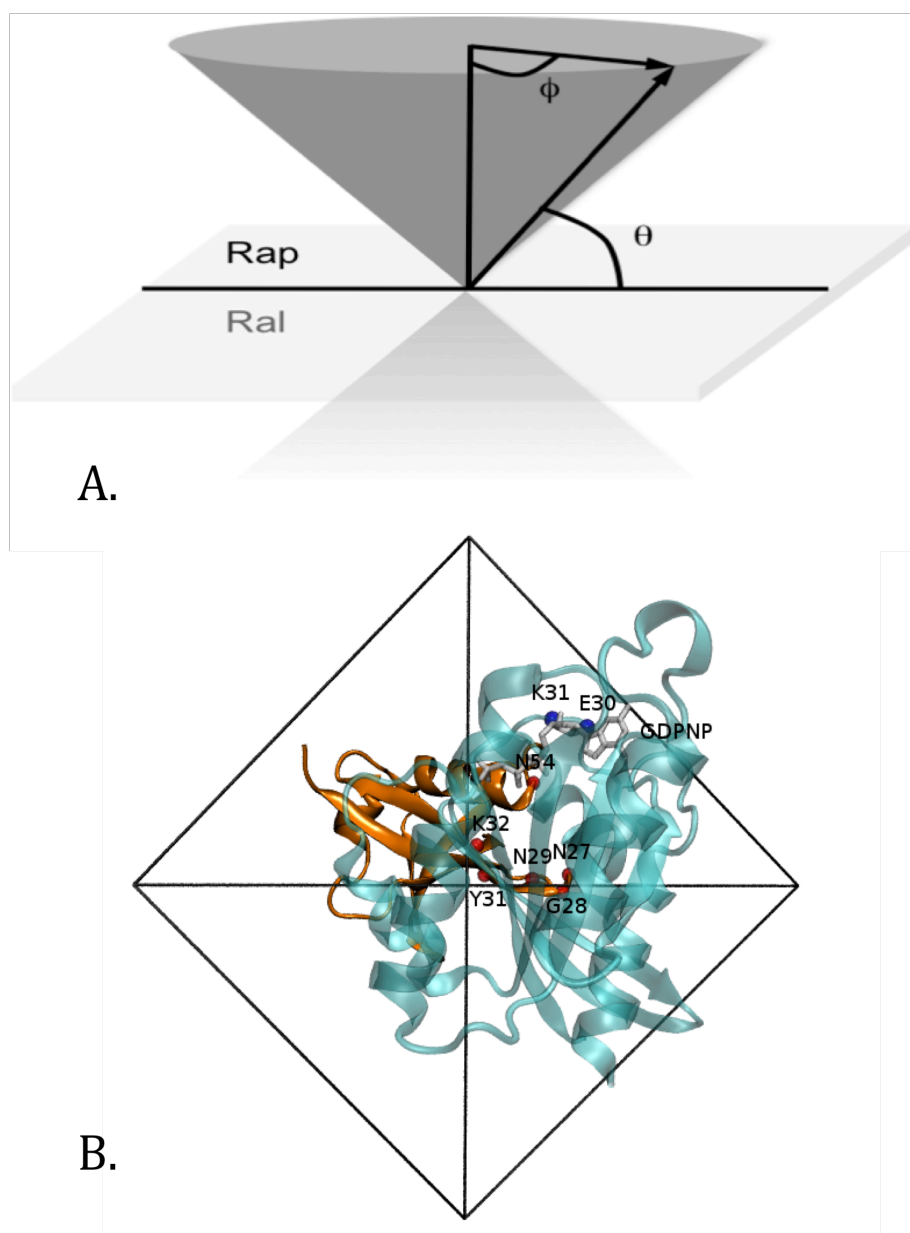
Figure 3.2. Representation of the azimuthal (*θ*) and polar (*ϕ*) angles for the residues discussed here. **A:** The surface plane was defined by the average of the plane fit with all Cα atoms. Azimuthal angles are shown relative to this plane, where Rap is above the plane and Ral is below the plane. **B:** Representation of the polar angle. Translating the black cross hairs to the Cα of each residue (represented by spheres) determines the origin of the polar angles presented in Figures 3.3 and 3.4. Rap is shown in blue and Ral in orange. Figure prepared by Mr. Ritchie.
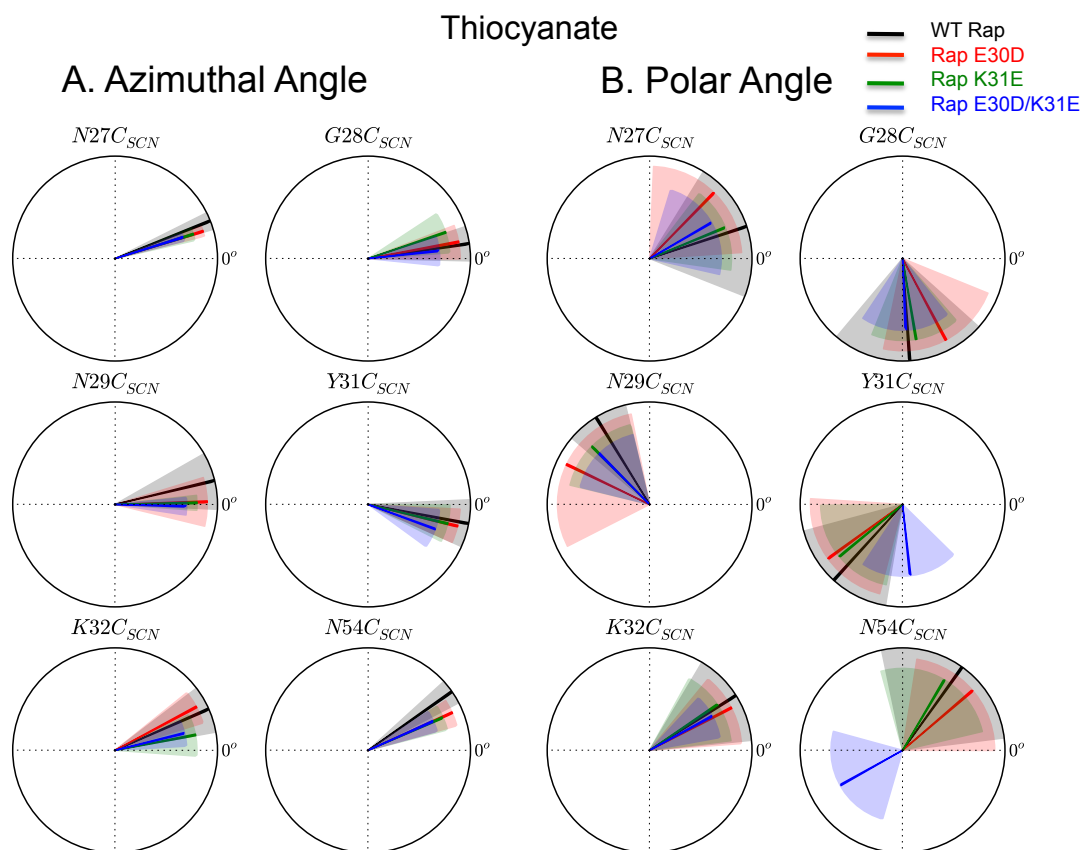
Figure 3.3. A. Azimuthal and B. polar angles of the thiocyanate on SCN-labeled Ralβ mutants calculated from each mutant docked with WT Rap (black), Rap E30D (red), Rap K31E (green), and Rap E30D/K31E (blue). Azimuthal angles are shown relative to the Rap-Ralβ surface plane. Polar angles are shown relative to the coordinate system described in Figure 3.2B. The shaded area represents one standard deviation on the calculated angle from the Boltzmann-weighted ensemble of structures. Data and figure prepared by Mr. Ritchie.
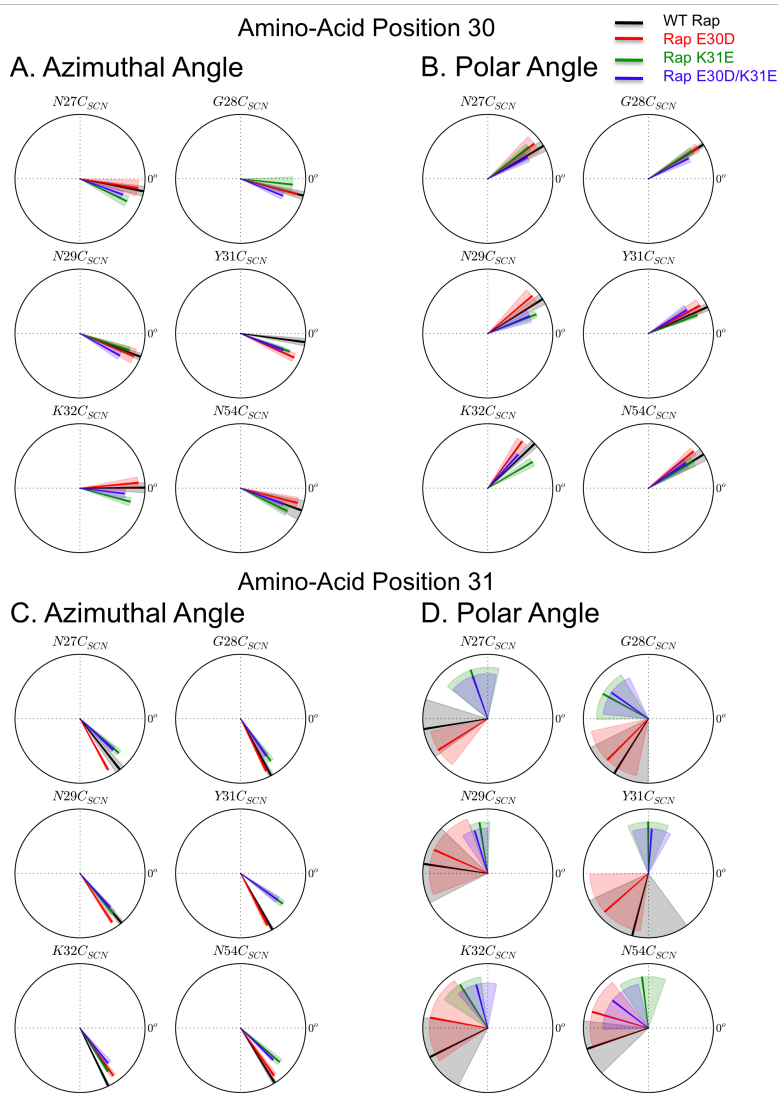
Figure 3.4. Azimuthal and polar angles of the side chain at Rap positions 30 and 31 in WT Rap (black), Rap E30D (red), Rap K31E (green), and Rap E30D/K31E (blue). **A:** Azimuthal angle at Rap position 30; **B:** polar angle at Rap position 30; **C:** azimuthal angle at Rap position 31; **D:** polar angle at Rap position 31. Azimuthal angles are shown relative the Rap-Ral surface plane. Polar angles are shown relative to the coordinate system shown in Figure 3.2B. The shaded area represents one standard deviation on the calculated angle from the Boltzmann-weighted ensemble of structures. Data and figure prepared by Mr. Ritchie.

34

together, the data strongly supports the evidence that mutations at Rap K31 are most important for causing structural changes that might affect Rap binding to the downstream effector Ral, and that mutations to Rap E30 do not significantly affect the structure of either WT Rap or Rap K31E. Both of these observations are consistent with differences in K_d between WT and mutated Rap binding to the downstream effector Ral.

Mr. Ritchie investigated the causes of the difference in orientation between the lysine and glutamate side chains at Rap position 31 through inspection of representative MD snapshots collected from sampling trajectories. This clearly revealed that when a lysine was at position 31, it pointed towards a hydrogen-bonding acceptor pocket formed by Ralβ D51, N54, and E58. When this side chain was mutated to Rap K31E in either the single or double mutant, the negatively charged glutamic acid reoriented to avoid electrostatic repulsion with this hydrogen-bond accepting pocket. This appears to be the central cause for both the dissociation constant and electrostatic differences between Rap-Ralβ binding and Ras-Ralβ binding described here. Although N54C$_{SCN}$ broadly followed this pattern, the orientation of the residue at position 31 in K31E and E30D/K31E varied more significantly than with the other mutants. Inspection of MD structures showed that when the nitrile probe was located at N54C$_{SCN}$, the nitrile disrupted the hydrogen-bonding pocket sufficiently to cause this portion of the Ralβ surface to retract slightly from the Rap-Ralβ interface, leaving K31 without these hydrogen bonds. Although the importance of this hydrogen-bonding pocket can be hypothesized from the 1LFD crystal structure,[29] this MD sampling has provided the first confirmation of the observed biochemical behavior of Ras and Rap with direct structural evidence.

Furthermore, Mr. Ritchie performed control simulations on the unmutated Ralβ docked with WT Rap and each Rap mutant to determine the effect that the cyanocysteine

35

mutation might have on the overall structure of the docked complex. He compared two general measurements of the structure around each mutated residue to the control simulations, the number of hydrogen bonds and the backbone root mean squared deviation (RMSD) for residues within 20 Å of the site's Cα. Both Ralβ mutants and their associated Ralβ WT simulations have the same number of protein-protein hydrogen bonds within the variance of the simulated Boltzmann-weighted ensemble. It is interesting to note that Ralβ N54 and N54C$_{SCN}$ show a systematic difference, which although it is still within error, is larger than other positions. As discussed, this is caused by the disruption that the N54C$_{SCN}$ mutant causes to the hydrogen-bonding interaction with Rap K31 in the docked complex, and is therefore expected. Significant changes in the backbone RMSD of any part of the protein system upon introduction of the cyanocysteine mutant would indicate large-scale differences in the structure of the protein within the docked complex. All RMSDs agreed within the standard deviation of the ensemble simulation. These control simulations demonstrate that the MD-generated ensemble of structures of the SCN-containing Ralβ complex do not have significant structural differences from simulations containing the WT residue at each location of interest.

3.3 VSE SPECTROSCOPY OF THE DOCKED PROTEIN-PROTEIN COMPLEX

3.3.1 Ralβ N27C$_{SCN}$ and Ralβ N29C$_{SCN}$

The selection of six SCN-labeled Ralβ probes was based on the consideration of each probes' orientation compared to the Rap-Ralβ interface, proximity to the Rap positions 30 and 31, and large differences in vibrational absorption energy upon binding to WT Ras and WT Rap measured in a previous study.[6] N27C$_{SCN}$ and N29C$_{SCN}$ were selected for probe locations because the Boltzmann-weighted molecular dynamics

simulations of the orientations of the six thiocyanate probes when docked with each of the Rap constructs determined that the thiocyanate group on these two Ralβ mutants had some of the largest angles with respect to the plane of the WT Rap-Ralβ interface of any of our probes, approximately 20-30° above the surface plane.[6] Because VSE spectroscopy is only sensitive to changes in the electrostatic field vector projected onto the nitrile bond axis, and because mutations to Rap K31 were themselves close to perpendicular to the Rap-Ralβ surface plane, probes perpendicular to the Rap-Ralβ plane would be most sensitive to mutations to Rap K31.

An example of the VSE data collected here is shown in Figure 3.5. The Ralβ N29C$_{SCN}$ mutant was incubated with each Rap mutant, concentrated, and the absorption energy of the nitrile probe was recorded and compared with the measured absorption energy when bound to WT Rap from a previous study.[6] When docked with Rap E30D, the thiocyanate absorption energy was 2160.8 cm^{-1}, identical to the observed absorption energy when Ralβ N29C$_{SCN}$ was bound to WT Rap. When Ralβ N29C$_{SCN}$ was incubated with Rap K31E, the absorption energy increased by 0.6 cm^{-1} to 2161.4 cm^{-1}. However, when docked with the double mutant, Rap E30D/K31E, the absorption energy of the thiocyanate shifted 0.8 cm^{-1} higher in energy (2161.6 cm^{-1}). Both Rap mutants containing K31E were therefore more similar to the observed absorption energy when Ralβ N29C$_{SCN}$ is docked with WT Ras (2161.1 cm^{-1}) than with WT Rap. This indicates that the probe is experiencing an electrostatic environment in the double mutant E30D/K31E that is more like that of WT Ras than WT Rap. The absorption energies for the SCN-labeled Ralβ mutants bound to the Rap constructs are summarized in Table 3.2 and Figure 3.6. In this table and figure, Δv_{obs} are referenced to the absorption energy of the nitrile probe when

37
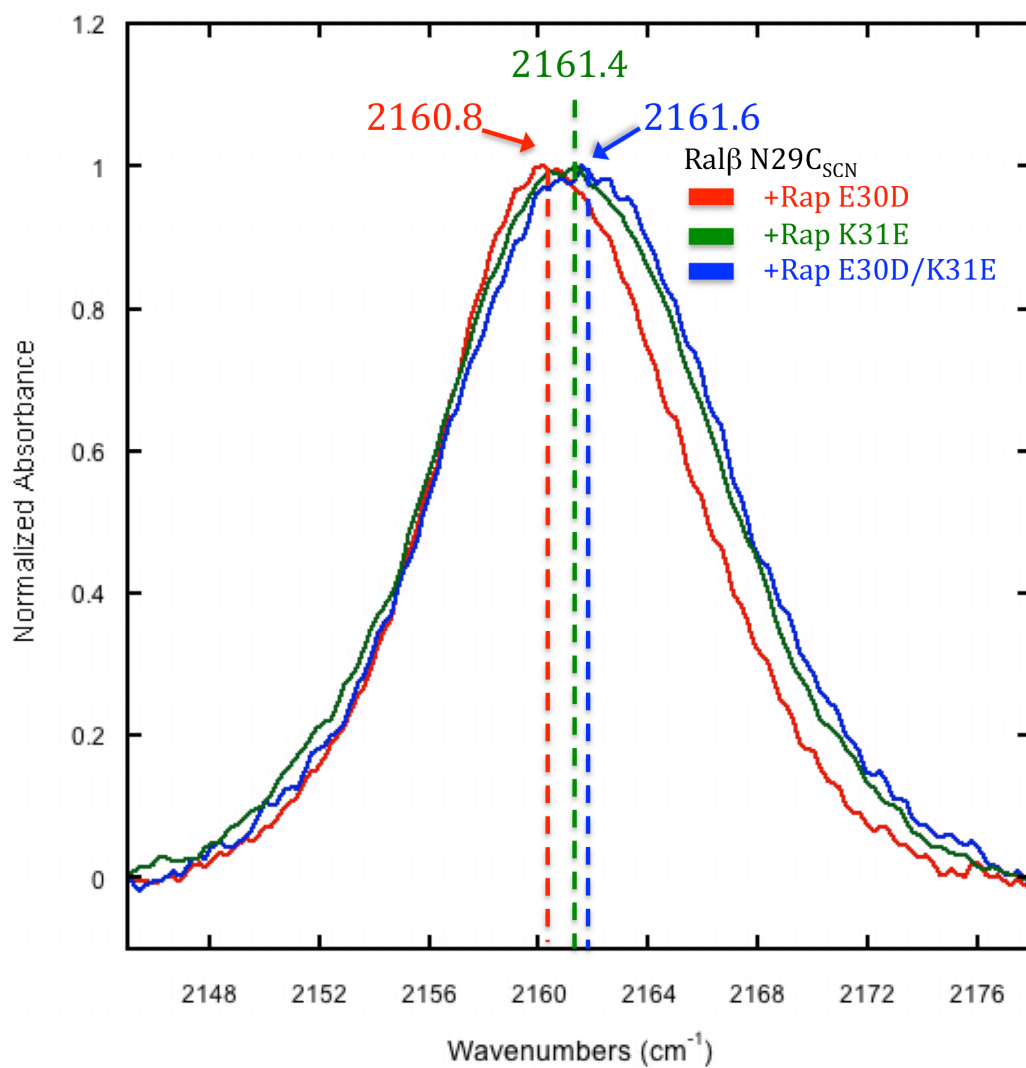
Figure 3.5. Normalized absorbance of thiocyanate on Ralβ N29C$_{SCN}$ measured when docked with Rap E30D (red, 2160.8 cm^{-1}), Rap K31E (green, 2161.4 cm^{-1}), and Rap E30D/K31E (blue, 2161.6 cm^{-1}).

Table 3.2.　Measured vibrational frequencies (v_{obs}) of SCN-Labeled Ralβ mutants docked with WT Rap; the observed changes in vibrational frequency (Δv_{obs}) upon docking each probe to WT Ras, Rap E30D, Rap K31E, and Rap E30D/K31E.　Error is reported as one standard deviation from multiple experiments.

GTPase		Ralβ Mutant					
		N27C	G28C	N29C	Y31C	K32C	N54C
WT Rap	v_{obs} (cm-1)	2162.6 ± 0.4	2161.8 ± 0.1	2160.8 ± 0.2	2161.5 ±0.2	2160.9 ± 0.2	2161.4 ± 0.2
		Difference Compared to WT Rap					
WT Ras	Δv_{obs} (cm-1)	-0.5 ± 1.0	-0.8 ± 0.1	0.3 ± 0.4	-0.8 ± 0.4	0.7 ± 0.8	-0.5 ± 0.4
Rap E30D	Δv_{obs} (cm-1)	-0.1 ± 0.4	1.0 ± 0.5	0.0 ± 0.2	-2.0 ± 0.4	-0.2 ± 0.6	0.4 ± 0.3
Rap K31E	Δv_{obs} (cm-1)	-0.6 ± 0.6	0.5 ± 0.2	0.6 ± 0.2	-1.0 ± 0.4	-1.0 ± 0.2	-0.1 ± 0.3
Rap E30D/K31E	Δv_{obs} (cm-1)	-0.3 ± 0.5	0.2 ± 0.3	0.8 ± 0.2	-0.2 ± 0.4	-1.2 ± 0.4	0.2 ± 0.3
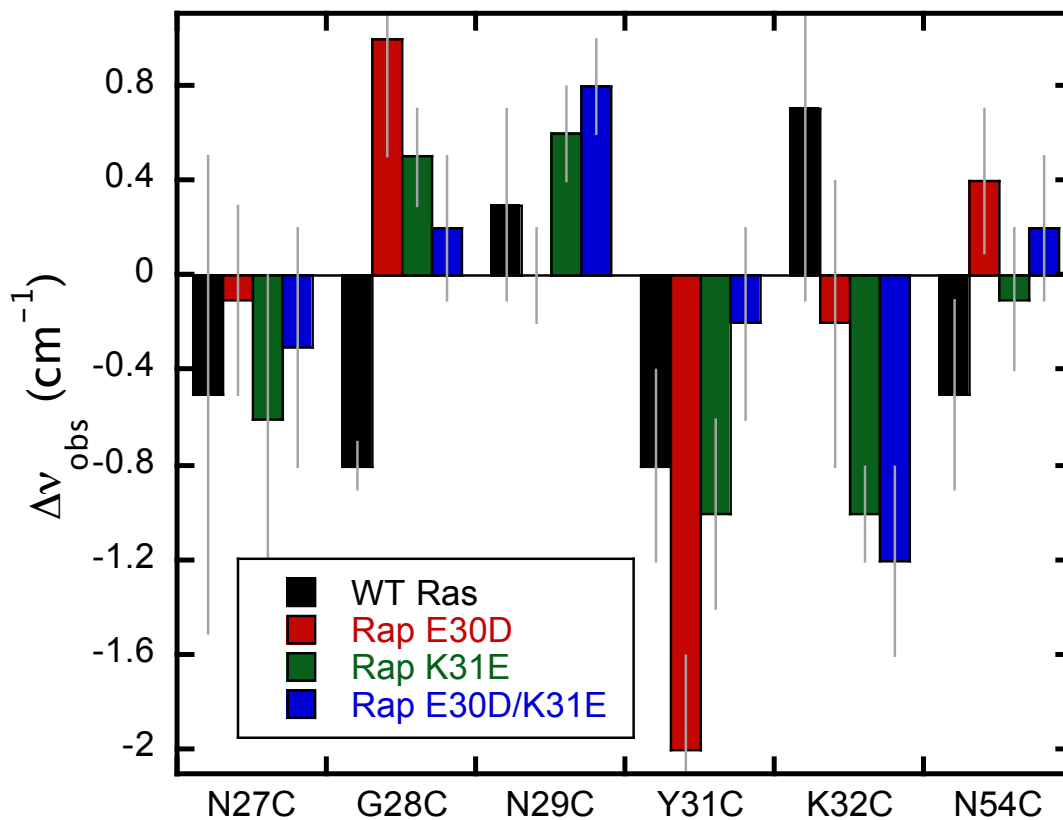
Figure 3.6. Change in absorption energy compared to WT Rap, $\Delta\nu_{obs}$, of the thiocyante on SCN-labeled Ralβ mutants when bound to WT Ras (blue), Rap E30D (red), Rap K31E (green), and Rap E30D/K31E (blue) where $\Delta\nu_{obs} = 0$ represents no change from the thiocyanate absorption energy when bound to WT Rap reported in Table 3.2. Error bars represent propagation of error of ν_{obs}.

docked with WT Rap (i.e. $\Delta v_{obs} = 0$ represents no change from the thiocyanate absorption energy when docked with WT Rap).[6]

When the probe is located at Ralβ N27C$_{SCN}$ and N29C$_{SCN}$, the data in Figure 3.6 clearly shows that both the single and double reversion mutants Rap K31E and E30D/K31E have nitrile absorption energies that are similar to WT Ras, not WT Rap. In both cases, the single mutation Rap E30D appears to have a negligible effect on the electrostatic environment of the probe. At these particular probe locations, therefore, the double mutation does indeed revert the electrostatic field of Rap back to that found in Ras. Although these energy shifts are small, the trend towards higher absorption energies when bound to WT Ras and the double mutant Rap E30D/K31E than when bound to WT Rap are clear. The relatively small effect of mutations on the magnitude of the absorption energy of Ralβ N29C$_{SCN}$ in particular may be due to the fact that the angle with respect to the Rap-RalGDS interfacial plane decreased for all Rap mutants relative to WT, possibly eliminating the utility of this probe position.

3.3.2 Ralβ K32C$_{SCN}$ and Ralβ N54C$_{SCN}$

The orientation of nitrile probes at positions K32C$_{SCN}$ and N54C$_{SCN}$ positioned them above and approaching perpendicular to the interfacial plane. These two residues are also near Rap positions 30 and 31 when the docked complex forms. The closest Ralβ amino acid to positions 30 and 31 is N54, (a distance from backbone atoms of approximately 11-16 Å in our Boltzmann-weighted ensemble of structures). As shown in Figure 3.6, the two single mutations E30D and K31E have small but opposite effects on the absorption energy of N54C$_{SCN}$ when compared to WT Rap; Rap E30D is 0.4 cm^{-1} higher in absorption energy, while Rap K31E is 0.1 cm^{-1} lower in absorption energy. The

combined effect of the double mutant Rap E30D/K31E, however, gave a VSE shift 0.2 cm^{-1} higher in energy than WT Rap, resulting in an absorption energy that was approximately the sum of the shifts caused by the two single mutations. As discussed above, because N54C$_{SCN}$ visibly disrupted the hydrogen-bonding interaction with Rap K31 in the docked complex, it is likely that the structural disruption of this interface means that this position is not appropriate for deconvoluting structural and electrostatic effects. This observation demonstrates the importance of investigating both structural and electrostatic contributions to the biochemical question of interest.

The nitrile vibrational probe was also placed at Ralβ K32C$_{SCN}$ because of its proximity to positions 30 and 31 on the GTPase in the docked complex. As can be seen in Table 3.2 and Figure 3.6, although the measured error in $\Delta\nu_{obs}$ was larger than other positions, there was a dramatic effect of the mutation Rap K31E on the absorption energy of the thiocyanate compared to WT Rap (-1.0 cm^{-1}), while Rap E30D caused only a small perturbation (-0.2 cm^{-1}). The behavior of the double mutant Rap E30D/K31E was the sum of these two shifts, -1.2 cm^{-1}. This was very different from the response on binding to WT Ras, which showed a shift in absorption energy of +0.7 cm^{-1} compared to WT Rap. These two probe locations responded to the double mutant Rap E30D/K31E essentially as the addition of electrostatic changes caused by each single E30D and K31E mutation. However, in neither case did the double reversion mutation to Rap produce an electrostatic environment measured by the probe that was similar to Ras.

3.3.3 Ralβ G28C$_{SCN}$ and Ralβ Y31C$_{SCN}$

We chose Ralβ G28C$_{SCN}$ as a probe location because it was between positions N27 and N29, even though it did not meet other desirable criteria. Previous studies had shown very little sensitivity to differences in binding to WT Ras *versus* WT Rap, and a

position in the docked complex that was more consistently parallel to the surface than either N27C$_{SCN}$ or N29C$_{SCN}$.[6] Even still, this probe did respond strongly to mutants Rap E30D and K31E (+1.0 cm^{-1} and +0.5 cm^{-1} *versus* WT Rap, respectively), compared to a shift of -0.8 cm^{-1} when bound to WT Ras. The double mutant, Rap E30D/K31E, however, only demonstrated a shift of +0.2 cm^{-1} compared to WT Rap. The probe at this location thus reacted in a manner in which the two single mutations appear to cancel each other out. After extensive inspection of our MD simulations, we have found no significant structural differences near G28C$_{SCN}$ to explain this observation. It could be that the distance between G28 and the region of the binding surface we are investigating by mutations at Rap E30 and K31 make Ralβ G28C$_{SCN}$ an ineffective probe for this study. This result is noteworthy, however, because the distance over which linear VSE effects can be accurately measured has still not been experimentally established.

Position Ralβ Y31C$_{SCN}$ was selected for study because the change in absorption energy upon docking to WT Rap differed from WT Ras by a large amount, 0.8 cm^{-1}. As shown in Table 3.2, both single mutants Rap E30D and Rap K31E shifted the absorption energy of the nitrile probe on Ralβ Y31C$_{SCN}$ to lower energy, by -2.0 cm^{-1} and -1.0 cm^{-1} respectively. However, the combined effect of the double mutant was to shift the absorption energy lower by only -0.2 cm^{-1} compared to WT Rap, substantially less than either single mutant. The MD simulations show that there is a significant reorientation of the side chain at position Rap 31 above and away from Ralβ Y31C$_{SCN}$ in the mutants Rap K31 and E30D/K31E, which likely cause this probe to become significantly less sensitive to the kinds of changes in electrostatic field in the binding region in which we are interested.

3.4 DISCUSSION

This study was motivated by functional observations that positions 30 and 31 of Ras and Rap, which are among the few chemical differences between the Ras and Rap interfaces, could help discriminate appropriate downstream effectors for each GTPase. Because of the structural similarities of these two protein surfaces, it is possible that downstream effector binding selectivity could be caused by changes in the electrostatic fields at the GTPase-effector interface caused by mutations at position 30 and 31, and in particular by the reversal of charge caused by the K31E mutation. Measuring this effect from the perspective of the downstream effector Ral, which can bind to both GTPases, proved useful to explore this aspect of GTPase function. Previous experimental work and extensive MD sampling provided us with criteria to guide the selection of positions for the nitrile probe on the Ralβ surface. These criteria were 1) angle of the nitrile with respect to the GTPase-effector interface, with probes perpendicular to the plane of the interface preferred (N27C$_{SCN}$ and N29C$_{SCN}$); 2) proximity to positions 30 and 31 when the docked complex is formed (K32C$_{SCN}$ and N54C$_{SCN}$); and 3) previously measured discrimination in absorption energy when docking to Ras as opposed to Rap, indicating those probes end up in significantly different electrostatic environments after the docked complex is formed (N27C$_{SCN}$, N29C$_{SCN}$, and Y31C$_{SCN}$). The location G28C$_{SCN}$ was chosen because of its position between N27C$_{SCN}$ and N29C$_{SCN}$, not because of any useful selection criteria, and could be considered as a control location on the Ralβ surface. No probe was an ideal experimental tool in all three of the selection criteria, and some probes were ideal in one experimental consideration but problematic in another. For example, the orientations of N27C$_{SCN}$ and N29C$_{SCN}$ in respect to the Rap-RalGDS interfacial plane were ideal, but the distances of these two probes from Rap positions 30 and 31 in the

docked complex were large. Even with detailed structural and electrostatic information, the limitations of the biological system does not allow us to design a perfect experiment; all probes will experience a convolution of ideal and problematic characteristics, and all probes will be unique. Electrostatic fields must therefore be explored from the perspectives of multiple probes, and information taken from the aggregation of the data.

We observed three general trends from the six probe locations studied. The first was seen with N27C_{SCN} and N29C_{SCN}, which displayed the Rap-to-Ras reversion behavior caused by the double mutation Rap E30D/K31E. The absorption energy of this double mutant essentially matched that of WT Ras, and in both cases was caused almost exclusively by the mutation K31E, not E30D. This is direct confirmation of hypotheses proposed from previous crystallographic and docking studies that the difference between Ras and Rap at these two positions leads to the functional discrimination these two GTPases have for different downstream effectors. The second observed trend was that of the double mutant displaying a difference in absorption energy that was simply the sum of the effect caused by the two single mutations. This was seen at positions K32C_{SCN} and N54C_{SCN}. This is strong experimental evidence that these mutations cause very little disruption in the docked complex, and experience additive changes in electrostatic field that can be measured by VSE spectroscopy of appropriately placed probes. However, it is important to study these effects from as many different probe locations as possible, because the third trend was less easily interpreted. For two probe locations, G28C_{SCN} and Y31C_{SCN}, while each single Rap mutation caused a large shift in vibrational absorption energy, the double mutant Rap E30D/K31E behaved essentially identically to WT Rap. No structural cause was found for this behavior. These residues may simply be unimportant for the formation of the Rap-Ral interface, and changes in electrostatic field

measured by probes at these locations may not be correlated with changes in Rap-Ral interface formation.

3.5 CONCLUSIONS

In summary, this study demonstrates that while VSE spectroscopy is a useful tool for examining molecular-level mechanism of electrostatic events in complex biological systems, the convolution of distance, orientation, and change in determining the change in local electrostatic field actually experienced by the nitrile probe needs to be carefully interpreted. Observation of reversion behavior in the double mutant Rap E30D/K31E with the probes Ralβ N27C$_{SCN}$ and N29C$_{SCN}$ strongly supports the role these two positions play in supporting an electrostatic mechanism of functional discrimination in GTPase-effector binding. Although these probe locations displayed the reversion mutation behavior that was predicted in the design of these experiments, the convolution of structure and sensitivity to mutations on the surface of Rap demonstrate that unambiguous measurement of electrostatic effects at the Rap-Ral interface will be difficult to achieve. Molecular dynamics sampling appears to be particularly useful in selection of appropriately placed VSE probes.

Chapter 4. Changes in Local Electrostatic Fields Caused by the Ras Mutations D30E and E31K Quantified by Vibrational Stark Effect Spectroscopy Create Rap-Like Docking to the Downstream Effector RalGDS

In the studies presented in this chapter, we systematically investigate the effect of the Ras reversion mutations D30E and E31K on the local electrostatic fields at the interface of the GTPases-RalGDS using vibrational Stark effect (VSE) spectroscopy, molecular dynamics (MD) sampling, and dissociation constant (K_d) measurements.[44] The thiocyanate (SCN) probe was incorporated at the same six locations used in Chapter 3 (N27, G28, N29, Y31, K32, and N54) plus an additional three locations (I18, R20, and S33) into the RalGDS interface. As previously mentioned, the probe locations were selected based on their use in a prior study that investigated the difference in the absorption energy of the SCN probe in the monomeric RalGDS protein compared to docked WT Ras and WT Rap.[6] The additional three locations were also part of this previous study. The locations selected for the SCN probe and the Ras side chains of interest are highlighted in Figure 4.1. Three of the SCN-probe locations, N27, N29 and Y31, have been hypothesized to be unique "hot spots" that could differentiate between two nominally identical proteins as their change in absorption energy has been different moving from monomer to bound complex for the WT Ras and WT Rap complexes. The Rap reversion (Chapter 3) work further supported this role of N27 and N29 as the absorption energy of the bound Rap double mutant complex strongly resembled the energy of the WT Ras bound complex.[17]

Each of the cysteine-less Ral (Ralβ) mutants containing the SCN probe was complexed with three Ras mutants: Ras D30E, Ras E31K and Rap D30E/E31K. The
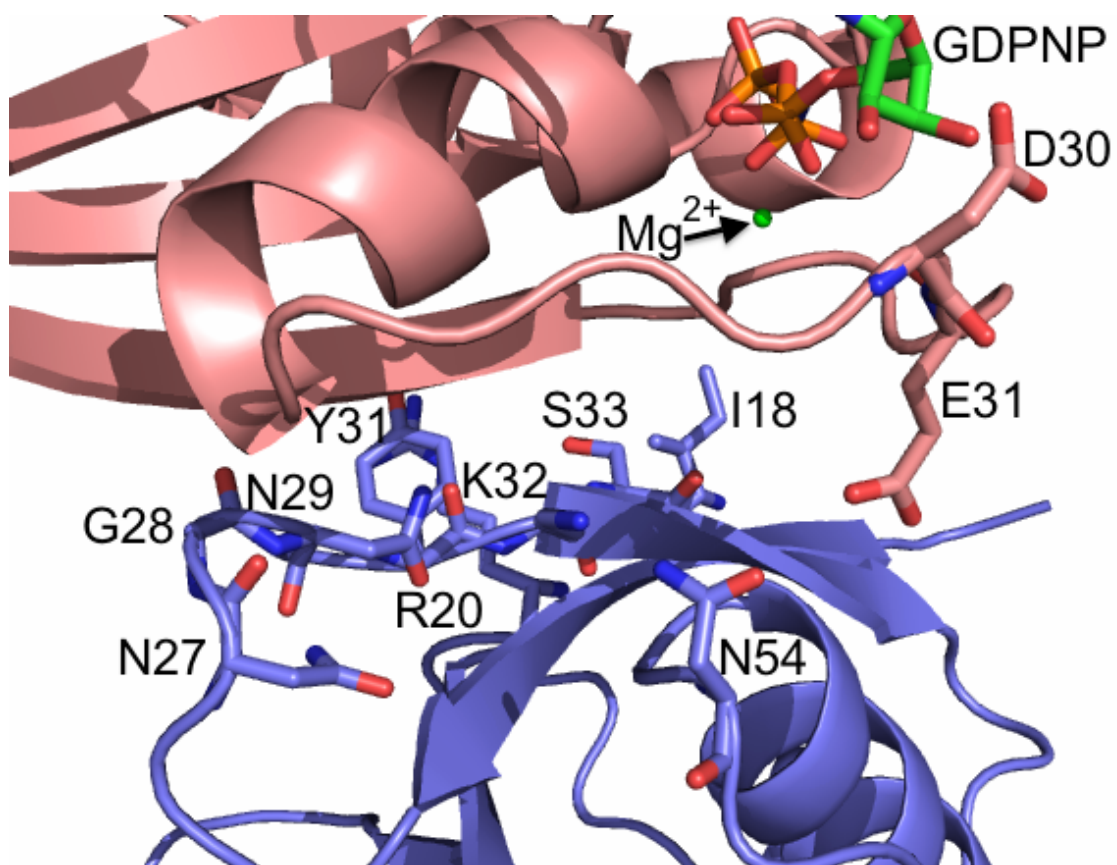
Figure 4.1. The Ras (salmon)-Ral (blue) interface from 1LFD[29], highlighting Ras D30 and E31 and nine amino acids on Ral that were selected for positioning the thiocyanate VSE probe in this study.

impact of the SCN probe on the binding interface of Ras/Ralβ interface was measured by gel chromatography and dissociation constant measurements. Only the probes at locations R20 and S33 were found to interrupt the Ras-Ralβ complex binding; the VSE and MD data for these probes is included but they were not further analyzed. The single mutation D30E was found to decrease the binding of RalGDS to WT Ras. Mr. Andrew Ritchie preformed extensive MD sampling of the SCN probe and the Ras 30 and 31 side chains to determine the Boltzmann-weighted orientations of the probe and side chains. The SCN-labeled Ralβ mutant's vibrational absorption energies, v_{obs}, was recorded and compared to the absorption energies docked to WT Ras and WT Rap from a previous study.[6] For all seven of the SCN-probe locations, at least one of the absorption energies of the Ras E31K and the Ras D30E/E31K complexes strongly resembled the energy when bound to WT Rap. Additionally, the single Ras mutant D30E was observed to yield large changes in absorption energy for four of the SCN probe locations. Mutations from aspartic acid to glutamic acid are normally considered conservative and benign, however, in this case the combination of the VSE and kinetics data suggest that the D30E mutation is unfavorable.

4.1 VERIFICATION OF BINDING

The effect of the incorporation of the SCN probe on the protein-protein interface can be determined by comparing differences in binding of the GTPase with SCN-labeled Ralβ mutants to the binding with WT Ral. Gel filtration chromatography clearly eluted a single Ras-Ral peak at the expected mass (~30 kDa) of the complex. The more quantitative dissociation constant measurement for each GTPase/RalGDS complex was measured using the guanine dissociation inhibition (GDI) assay and the results are summarized in Table 4.1. As expected, the WT Rap-WT Ral complex bound 10-times

more tightly than the WT Ras-WT Ral complex. As previously shown, except for Ralβ R20C$_{SCN}$ and Ralβ S33C$_{SCN}$ mutants, the removal of wild-type cysteines and introduction of the SCN probe does not significantly impact the binding of the RalGDS to Ras and qualitatively replicated the excepted differences in binding between the WT Ras and WT Rap bound complexes.[6,17] This result indicates that for the remaining seven SCN-labeled Ralβ mutants the cysteine mutagenesis and labeling were benign to the formation of the docked complexes. The data for the misbehaving Ralβ R20C$_{SCN}$ and Ralβ S33C$_{SCN}$ mutants are included throughout this study, but the results are not discussed further as the SCN probe at these locations disrupt the interaction with WT Ras before the added complication of the reversion mutations are considered.

Dissociation constants for the seven remaining probe locations binding to the three Rap reversion mutations studied here, Ras D30E, Ras E31K, and the double mutant Ras D30E/E31K, were then measured (Table 1). There are two significant conclusions from an examination of this data. First, the incorporation of E31K lowered the binding constant (K_d) of the Ras 31 mutants (Ras E31K and Ras D30E/K31E) to WT Ral as expected. Second, the mutation D30E was, in general, highly disruptive to the formation of the Ras E30D-Ralβ docked complex, causing up to a 10-fold increase in K_d for several of the probe locations (N27C$_{SCN}$, G28C$_{SCN}$, and N29C$_{SCN}$), and smaller although still substantial increases in K_d for WT Ral, Y31C$_{SCN}$, K32C$_{SCN}$, and N54C$_{SCN}$. For only one probe location, I18C$_{SCN}$, was there only minor effects on the magnitude of K_d for the D30E mutation compared to the WT Ral interaction. This is a surprising conclusion because the substitution of the aspartate for glutamate changes the size of the side chain by only a single methylene group, and is not predicted to alter pK_a values or sampling of structural degrees of conformational freedom about the amide backbone to any

50

Table 4.1.   Dissociation constant, K_d, of the formation of docked complexes of WT and
SCN-labeled Ralβ mutants with WT Ras, WT Rap, Ras D30E, Ras E31K
and Ras D30E/E31K. All values are reported in μM and errors represent
one standard deviation from multiple experiments.

Dissociation Constants (μM)					
Ral Monomer	WT Ras	WT Rap	Ras D30E	Ras E31K	Ras D30E/ E31K
WT Ral	1.4 ± 0.2	0.26 ± 0.09	5.9 ± 1.7	0.58 ± 0.15	1.8 ± 0.3
I18C	6.7 ± 1.8	0.07 ± 0.02	3.0 ± 0.9	1.7 ± 1.4	1.9 ± 0.2
R20C	3.1 ± 1.1	41 ± 16	2.9 ± 3.1	15.7 ± 2.3	11.2 ± 2.9
N27C	7.3 ± 2.2	0.30 ± 0.05	54.5 ± 28.9	2.3 ± 0.3	1.8 ± 0.6
G28C	4.8 ± 1.1	0.04 ± 0.004	97.1 ± 85.6	1.9 ± 0.9	0.64 ± 0.21
N29C	3.1 ± 0.6	0.15 ± 0.08	70.5 ± 28.4	3.8 ± 0.6	1.0 ± 0.2
Y31C	12.9 ± 4.8	1.0 ± 0.1	22.8 ± 2.1	7.6 ± 0.6	4.0 ± 0.5
K32C	6.0 ± 2.3	0.69 ± 0.18	15.5 ± 2.2	8.2 ± 0.8	3.5 ± 0.4
S33C	2.2 ± 0.4	1.3 ± 0.4	7.7 ± 3.3	4.1 ± 0.7	14.2 ± 2.2
N54C	4.7 ± 0.4	0.91 ± 0.20	5.1 ± 1.3	1.1 ± 0.4	0.5 ± 0.5

significant extent. To our knowledge, this effect has never before been observed in the GTPase-downstream effector studies.

4.2 MOLECULAR DYNAMICS

Understanding of the molecular geometry of the Ras/Ral system is important for the interpretation of VSE spectral data because the observed changes in the absorption energy serve as a reporter of change in the local electrostatic fields projected along the nitrile bond vector and therefore could be a convolution of electrostatic and structural factors. The x-ray crystal structure, 1LFD[29], was used as a starting point for the MD simulation of the Ras side chains 30 and 31 and the nitrile spectral probes. Although, the crystal structure gives valuable insight into the Ras/Ralβ interface, it only provides a single snapshot and no information about steady-state motions that influence the vibrational absorption energy measurements collected over several minutes. Furthermore, our exact experimental system contains a series of mutations including the mutation of the WT cysteines to alanines, the incorporation of the SCN probe as a cyanocysteine side chain and the Ras functional mutations. These mutations are not currently described by a crystal structure and so must be modeled into the system. Incorporation and movement of the SCN probe could be cause for experimental observations of vibrational absorption energy that have nothing to do with electric field, as we are interested in isolating here, and more to do with structural and steric factors, which is not our immediate interest. Therefore, Mr. Andrew Ritchie of the Webb group performed extensive molecular dynamics sampling of each SCN-labeled Ralβ mutant docked with WT Ras and the Ras mutants D30E, E31K, and D30E/E31K to accumulate a Boltzmann-weighted ensemble of

simulated orientations of the thiocyanate group and the side chains at Ras positions 30 and 31.[44]

Mr. Ritchie analyzed the Boltzmann-weighted probable orientations of the Ras side chains 30 and 31 and the SCN probe in our system. He defined 2 angles with respect to the Ras-Ral interface, an azimuthal angle (θ) and polar angle (ϕ), both described in Figure 4.2. As shown in Figure 4.2A, the angles are defined relative to an interfacial plane between Ras and Ral. In this orientation, an azimuthal angle of $\theta > 0$ indicates that the nitrile vector or the Ras side chain vector is pointed towards Ras, while $\theta < 0$ indicates that the oscillator or side chain is pointed to the Ralβ mutant. The polar angle (ϕ) describes the orientation of the nitrile oscillator with respect to the center of mass of the docked complex. Because the location of each simulated side chain will be different relative to the center of mass of the protein, when the crosshairs in Figure 4.2B are moved to the Cα (blue spheres) of the Ras side chains or the Cδ (red spheres) of the Ral SCN-probes, they indicate the origin of the polar angles shown in Figures 4.3 and 4.4. The azimuthal and polar angles for the Ras side chains and the SCN-probes are shown in Figure 4.3 and 4.4 respectively, with the variance determined from the Boltzmann-weighted ensemble of the structures shown as a shaded region about the ensemble average.

Similar to the Rap mutation findings from Chapter 3,[17] The azimuthal and polar angles for the Ras side chains and the SCN-probes are shown in Figure 4.3 and 4.4 respectively, with the variance determined from the Boltzmann-weighted ensemble of the structures shown as a shaded region about the ensemble average. As previously observed, the azimuthal angles (Figure 4.3 A and C) of either Ras residue at positions 30 and 31 did not vary significantly based on the mutant Ras of Ralβ construct being
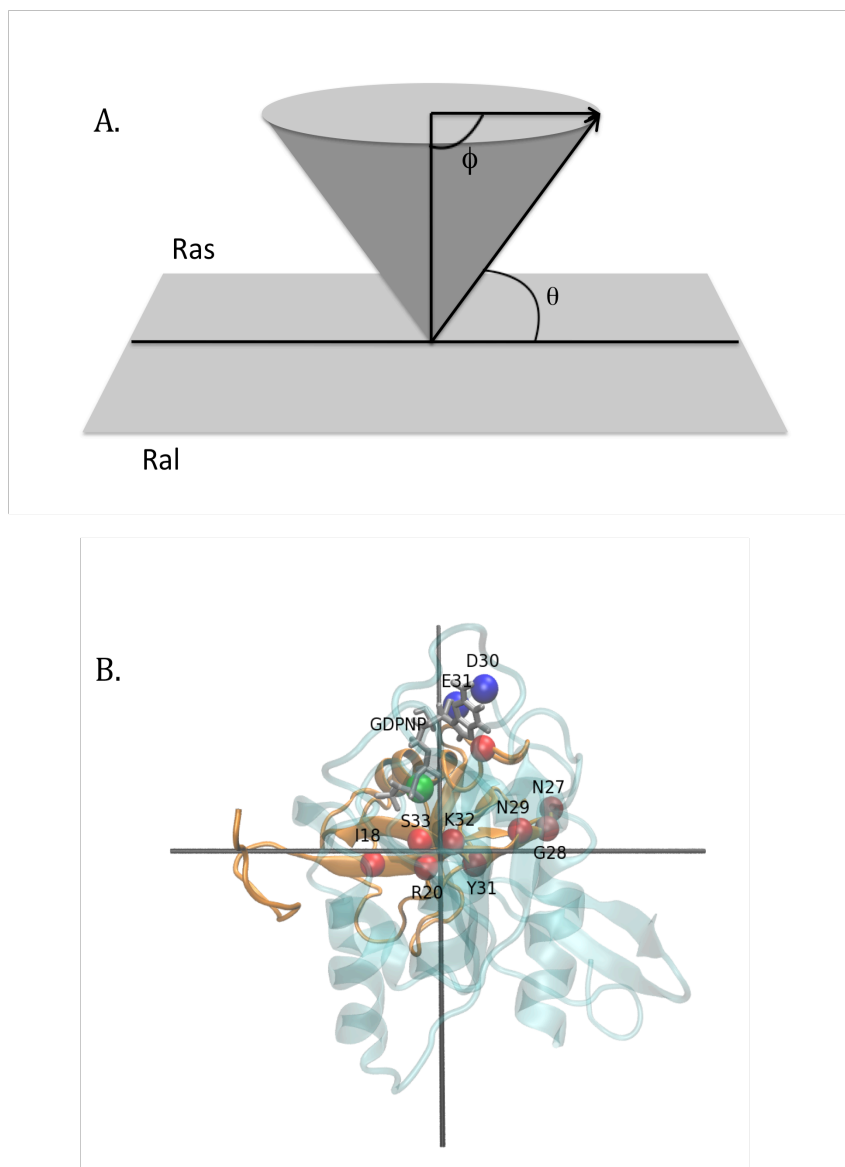
Figure 4.2. Representation of azimuthal (θ) and polar (φ) angles for the Ras side chains and SCN-probe. (A) The interfacial plane between Ras and Ral is indicated with Ras above and Ral below the surface. The azimuthal angles (θ) are relative to this plane with angles towards Ras defined as positive and towards Ral as negative. (B) Represents the origin of the polar angles. Translating the crosshairs to the Cα of the Ras side chain (blue sphere) and the Cδ of the Ral SCN-probe determine the origin of the polar angles in Figure 4.3 and 4.4. Figure 4.2 was prepared by Mr. Ritchie.

54

Ras Position 30

A. Azimuthal Angle

B. Polar Angle

Ras Position 31

C. Azimuthal Angle
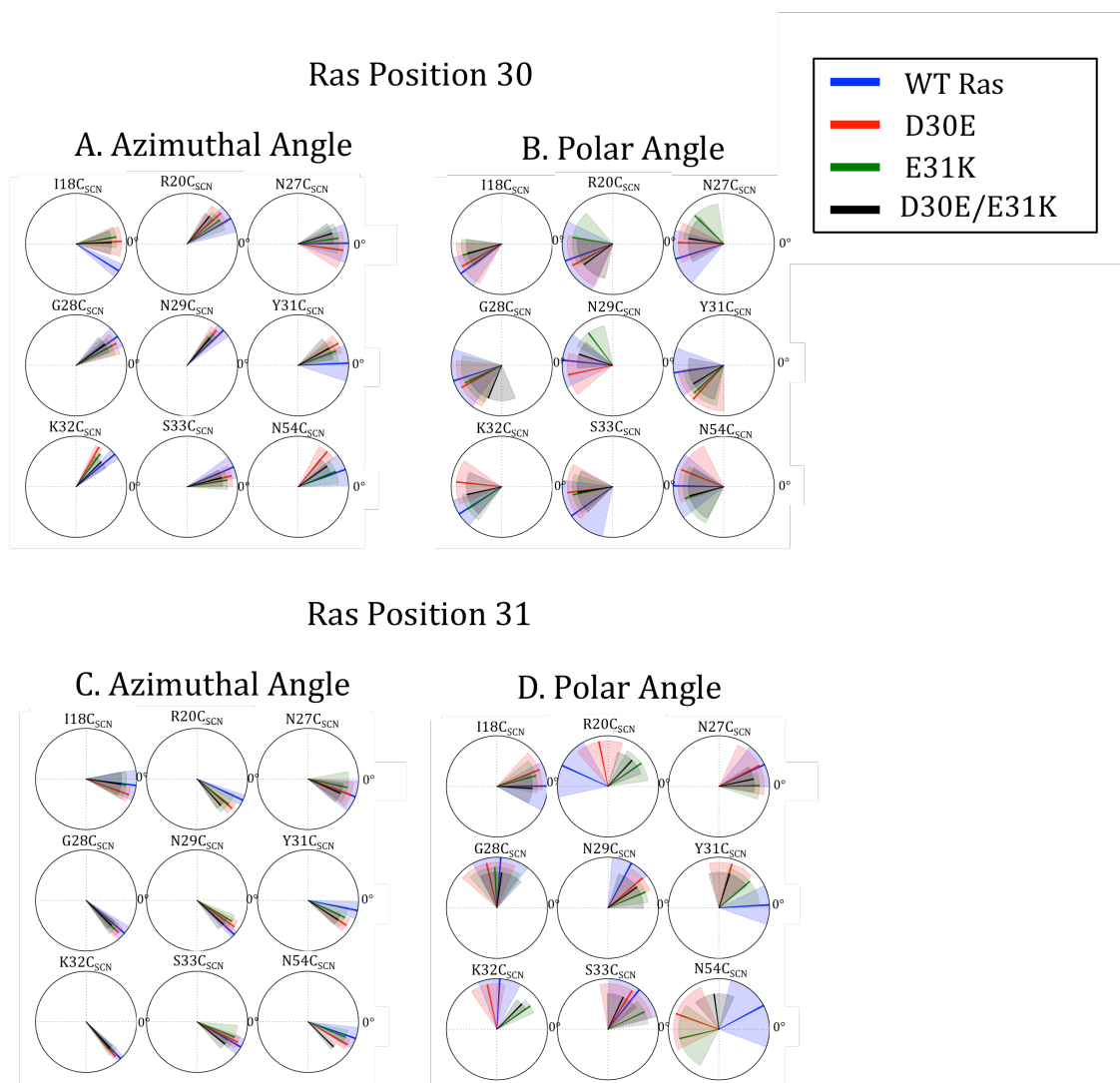
D. Polar Angle

Figure 4. 3. Azimuthal and polar angles of the Ras side chains in the GTPase-Ral bound complex with WT Ras (blue), Ras D30E (red), Ras E31K (green) and Ras D30E/E31K (black). (A) Azimuthal angle of Ras position 30. (B) Azimuthal angle at Ras position 31. (C) Polar angle at Ras position 30. (D) Polar angle at Ras position 31. Azimuthal angles are shown relative to the Ras-Ral interface and the polar angles are in reference to the coordinate system shown in Figure 4.2B. The shaded area represents the variance from the Boltzmann-weighted ensemble of structures.
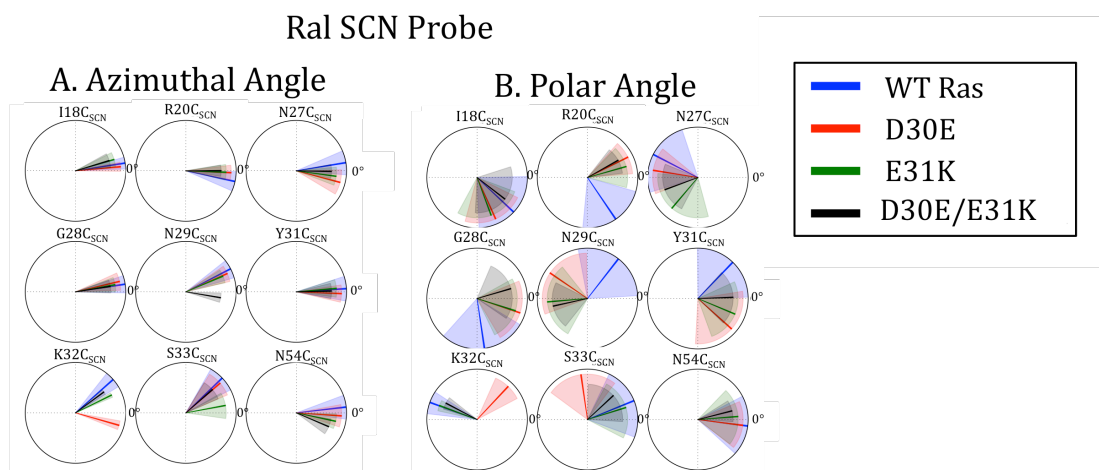
Figure 4. 4. Azimuthal and polar angles of the SCN probe in the GTPase-Ral bound complex with WT Ras (blue), Ras D30E (red), Ras E31K (green) and Ras D30E/E31K (black). (A) Azimuthal angle of the SCN probe. (B) Polar angle of the SCN probe. Azimuthal angles are shown relative to the Ras-Ral interface and the polar angles are in reference to the coordinate system shown in Figure 4.2B. The shaded area represents the variance from the Boltzmann-weighted ensemble of structures. Data and figure prepared by Mr. Ritchie.

studied. The polar angles (Figure 4.3 B and D) had greater movement over the MD trajectories, which can be seen from the larger variances. The polar angle of position 30 did not vary significantly based on the identity of the Ras or Ralβ mutant being studied. However, the identity of the Ralβ construct clearly impacted the polar angle of the residues at position 31. For example, the polar angles of the Ras 31 side chains are all approximately 0° when bound to Ralβ I18C$_{SCN}$ compared to approximately 90°complexed to Ralβ G28C$_{SCN}$. However, only in the cases of Y31$_{CSCN}$ and N54C$_{SCN}$ did the polar angle of the Ras 31 side chain vary significantly based on the Ras construct for a given Ralβ mutant. Similar to the Ras side chains, the azimuthal angles (Figure 4.4A) of each SCN-probe are approximately parallel to the Ras-Ral interface and were unaffected by the identity of the Ras constructs bound. The single exception to this observation was the SCN-probe on Ralβ K32C$_{SCN}$ docked to Ras D30E, which assumed an azimuthal angle of ~-10° compared to ~15°when docked to any other Ras construct. The absolute differences in the SCN-probe polar angles (Figure 4.4B) cannot be easily compared between Ralβ complexes as based on the way the polar angle is defined, the differences simply indicate different origins within the protein. Once again, the only SCN-probe sensitive to the identity of the bound Ras construct is the Ralβ K32C$_{SCN}$ mutant docked to Ras D30E, where the polar angle is ~45° bound to Ras D30E compared to ~170° bound to any of the Ras construct.

4.3 VIBRATIONAL STARK EFFECT SPECTROSCOPY

The locations selected for the 9 spectral probes on the Ras binding domain (RBD) of RalGDS were selected from a previous study.[6,17] The IR spectra for the nine VSE spectral probes for the 27 Ralβ probe/Ras mutant combinations were measured and recorded. Example spectra for Ralβ Y31C$_{SCN}$ bound to Ras E31K (green, 2161.7 cm^{-1})

and Ras D30E/E31K (black, 2160.2 cm^{-1}) are shown in Figure 4.5. Each spectrum was fit using in-house software to determine the center and full width at half maximum (fwhm) of each absorption peak.[17] These are summarized in Table 4.2, with standard deviations reported from a minimum of four measurements. The change in absorption energy and fwhm caused by the Ras mutation on the SCN-labeled Ralβ mutant in the Ras/Ralβ was determined by comparing the absorption energy and fwhm of the probe in the mutant complex to its energy and fwhm in the WT Ras/Ralβ complex.   The differences between these values when docked to WT *versus* mutant Ras are shown in Figure 4.6. In this figure, the extent to which the reversion mutations replicate the electrostatic environment of the SCN probe bound to WT Rap would appear as a difference in absorption energy, Δv_{obs}, that is similar in both magnitude and direction to the WT Rap complex (orange). As mentioned previously, we include data for all nine-probe locations, even though two locations, R20C$_{SCN}$ and S33C$_{SCN}$, are not expected to demonstrate reversion behavior due to inconsistencies in K_d.

   We initiated this work to test the hypothesis that the mutations at positions 30 and 31 of the GTPase, and most importantly the charge-altering K31E mutation, were primarily responsible for Ral's ability to select Ras *versus* Rap *in vitro*, as has been demonstrated with previous Rap reversion mutants studied through both kinetic and electrostatic methods. As the data in Figure 4.6 demonstrate, this effect was substantially confirmed by all seven of the remaining well-behaved SCN-labeled Ralβ constructs. At all of these probe locations, docking to Ras E31K (green) and/or the double mutant Ras D30E/E31K (black) caused a change in the absorption energy of the thiocyanate of the same direction and similar magnitude as docking with WT Rap (orange). The most striking example of this is I18C$_{SCN}$, for which the double mutation and docking to WT
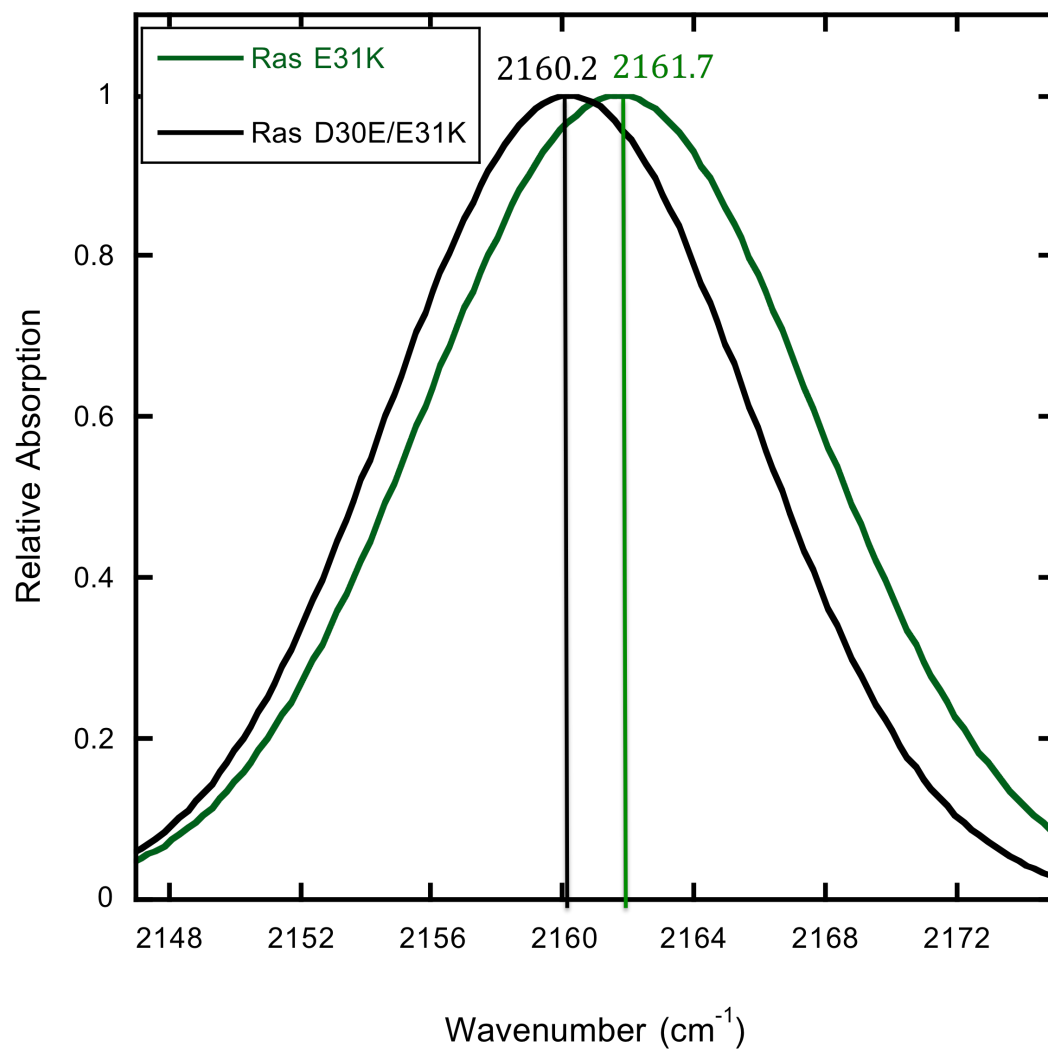
Figure 4.5.   Normalized, fitted absorption of the thiocyanate on Ralβ Y31C$_{SCN}$ measured when docked to Ras E31K (green, 2161.7 cm^{-1}) and Ras D30E/E31K (black, 2160.2 cm^{-1}).

Table 4.2.   Measured absorption frequencies ν_{obs} (cm^{-1}) and full-width half maximum (fwhm, cm^{-1}) of the SCN-labeled Ralβ mutants docked to the WT Ras, WT Rap, Ras D30E, Ras E31K and Ras D30E/E31K. Error is reported as one standard deviation from multiple experiments.

Ral Monomer		WT Ras	WT Rap	Ras D30E	Ras E31K	Ras D30E/ E31K
I18C	ν_{obs} (cm^{-1})	2162.8 ± 0.2	2162.1 ± 0.1	2162.3 ± 0.1	2163.0 ± 0.1	2162 ± 0.2
	fwhm (cm^{-1})	12.8 ± 0.5	13.3 ± 0.5	13.3 ± 0.1	12.7 ± 0.6	13.2 ± 0.2
R20C	ν_{obs} (cm^{-1})	2162.5 ± 0.1	2161.9 ± 0.2	2161.2 ± 0.1	2162.3 ± 0.2	2161.1 ± 0.1
	fwhm (cm^{-1})	12.3 ± 0.2	12.3 ± 0.5	15.2 ± 1.0	14.5 ± 0.8	14.5 ± 0.7
N27C	ν_{obs} (cm^{-1})	2162.8 ± 0.2	2162.6 ± 0.4	2162.6 ± 0.2	2162.3 ± 0.5	2162.8 ± 0.1
	fwhm (cm^{-1})	13.5 ± 0.8	14.1 ± 0.4	12.8 ± 0.1	12.9 ± 1.6	12.8 ± 0.2
G28C	ν_{obs} (cm^{-1})	2161.0 ± 0.1	2161.8 ± 0.1	2160.2 ± 0.2	2161.9 ± 0.3	2160.5 ± 0.3
	fwhm (cm^{-1})	14.1 ± 0.5	13.6 ± 0.8	13.1 ± 0.7	14.5 ± 1.3	19.3 ± 3.1
N29C	ν_{obs} (cm^{-1})	2161.1 ± 0.3	2160.8 ± 0.2	2161.6 ± 0.4	2161.2 ± 0.2	2161.0 ± 0.1
	fwhm (cm^{-1})	14.0 ± 0.2	12.8 ± 1.1	14.4 ± 0.3	13.3 ± 0.7	13.4 ± 1.0
Y31C	ν_{obs} (cm^{-1})	2160.7 ± 0.3	2161.5 ± 0.2	2161.5 ± 0.1	2161.7 ± 0.1	2160.2 ± 0.2
	fwhm (cm^{-1})	14.1 ± 0.6	13.5 ± 1.0	13.8 ± 0.2	13.8 ± 0.2	13.9 ± 0.6
K32C	ν_{obs} (cm^{-1})	2162.1 ± 0.3	2160.9 ± 0.2	2160.0 ± 0.3	2161.6 ± 0.1	2161.7 ± 0.1
	fwhm (cm^{-1})	15.0 ± 1.2	15.9 ± 0.7	16.1 ± 1.6	13.4 ± 0.4	13.2 ± 0.2
S33C	ν_{obs} (cm^{-1})	2161.0 ± 0.1	2161.0 ± 0.1	2162.0 ± 0.1	2161.6 ± 0.2	2161.5 ± 0.1
	fwhm (cm^{-1})	15.0 ± 1.0	13.4 ± 1.0	15.2 ± 0.2	14.8 ± 0.4	14.2 ± 0.2
N54C	ν_{obs} (cm^{-1})	2160.9 ± 0.4	2161.4 ± 0.2	2162.3 ± 0.1	2162.0 ± 0.1	2161.8 ± 0.2
	fwhm (cm^{-1})	12.7± 0.2	13.5 ± 0.3	12.6 ± 0.5	12.7 ± 0.2	12.4 ± 0.5
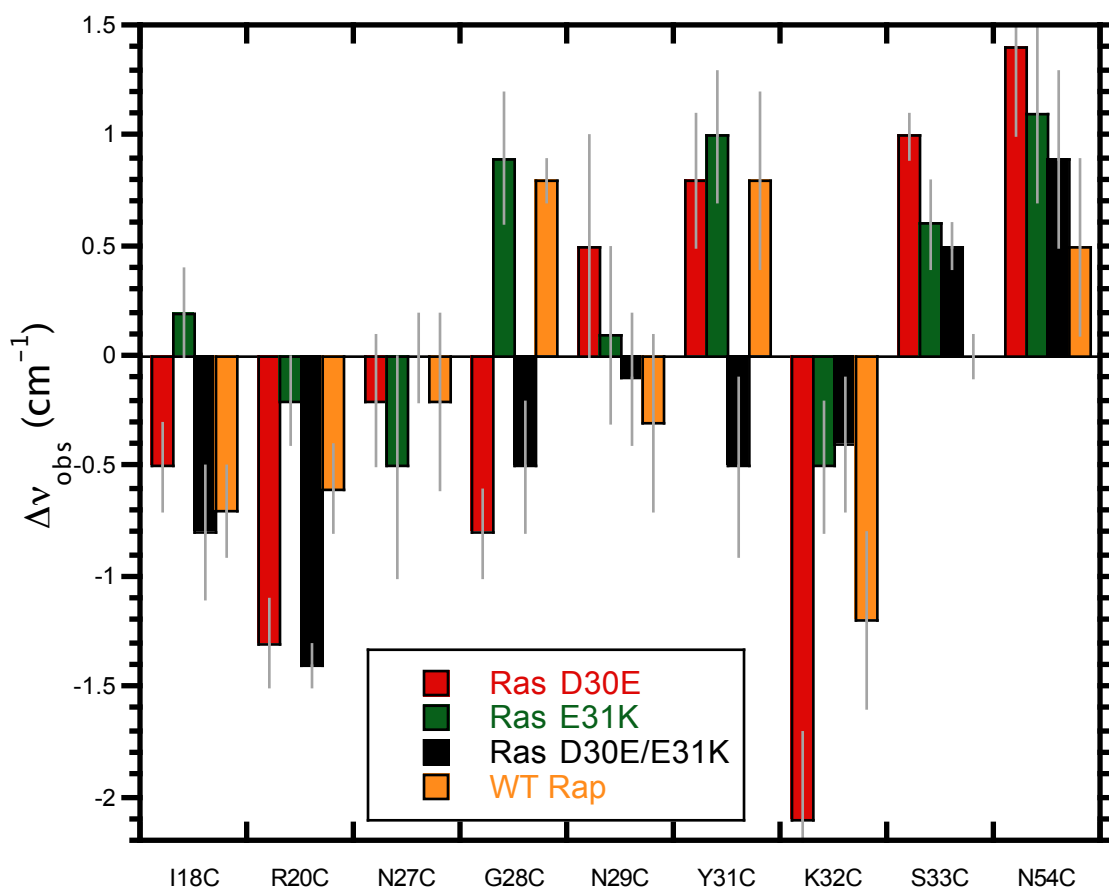
Figure 4.6. Change in absorption energy compared to WT Ras, Δv_{obs}, of the thiocyanate on the SCN-labeled Ralb mutants when docked to Ras D30E (red), Ras E31K (green), Ras D30E/E31K (black) and WT Rap (orange), where $\Delta v_{obs} = 0$ no change from the thiocyanate absorption energy when bound to WT Ras reported in Table 4.2. Error bars represent propagation of error of v_{obs}.

Rap created changes in absorption energy that were essentially identical (2162.1 cm^{-1} and 2162.0 cm^{-1}, respectively), and G28C$_{SCN}$, for which charge-reversal mutation Ras E31K and WT Rap created changes in absorption energy that were essentially identical (2161.9 cm^{-1} and 2161.8 cm^{-1}, respectively). Although this trend was less dramatic at the other five positions, the change in absorption energy of the SCN probe docked to Ras E31K or Ras D30E/E31K was within standard deviation of the WT Rap complex indicating that the E31K or the D30E/E31K combination mutations appeared to be partly or fully responsible for changes in electrostatic fields that complemented the functional results determined by measuring the dissociation constant of the docking interaction.

The results for dissociation constant of the Ras D30E given in Table 4.1 clearly show that this mutation does not convey "reversion" behavior. The difference between Ras and Rap at this position has been assumed to be benign because of the relatively conservative change made when substituting one acid for another. However, our data demonstrates that for the 7 probe locations, the D30E mutation caused a significant increase in K_d, and thus represented a mutation that destabilized the formation of the protein-protein complex. This result was also observed for WT Ral docking with Ras D30E, demonstrating that this was an effect of the mutation on the GTPase, not the mutation and SCN-label on the downstream effector. In light of this functional result, it is particularly interesting to examine the effect of the Ras D30E mutation on spectral changes to each SCN-containing Ralβ probe. A significant and surprising trend seen in Figure 4.6 is that over half of our SCN-probe locations, I18C$_{SCN}$, R20C$_{SCN}$, N27C$_{SCN}$, Y31C$_{SCN}$, and K32C$_{SCN}$, the absorption energy of the nitrile is strongly affected by the mutation D30E compared to WT Ras. Additionally, the orientation of the Ralβ K32C$_{SCN}$ probe location bound to the Ras D30E mutation deviates greatly from the angles of the

probe bound to any other Ras complex. The Ras D30E-Ralβ K32C$_{SCN}$ had the largest change in absorption energy measured (-2.1 cm^{-1}), which is likely due to a convolution of structural and electrostatic factors. The impact of the Ras D30E mutation of K_d and the observed absorption energies is surprising because these two residues differ by only a single methylene unit, and because to the best of our knowledge, no previous studies on this position have observed this effect.

4.4 CONCLUSIONS

The Ras mutation study further supported the important role of the amino acid 31 in the binding discrimination differences of RalGDS for Rap over Ras. Two of the SCN-probe locations, R20C and S33C, decreased the binding of RalGDS to WT Ras. For the remaining 7 locations, the absorption energy of at least one of Ras E31K and Ras D30E/E31K strongly resembled the absorption energy of the SCN-labeled Ralβ-WT Rap complex. Additionally, both the VSE and kinetics data demonstrated that the Ras D30E mutation was unfavorable, negatively impacting the RalGDS-Ras binding interface. This observation was surprising, as the mutation from aspartic acid to glutamic acid is typically considered conservative and benign as the two amino acids only differ by one methylene group. The largest change in absorption energy of the study was Ras D30E-Ralβ K32C$_{SCN}$ compared to the WT Ras complex. Additionally, the SCN probe of Ralβ K32C$_{SCN}$ complexed with Ras D30E was in a dramatically difference orientation than when complexed with the other Ras variants. The combination of the MD and VSE data for Ras D30E-Ralβ K32C$_{SCN}$ demonstrated the need for probe structural information to deconvolute structural and electrostatic factors when interpreting VSE spectral data.

Chapter 5. Exploring the Effect of Solvent Dielectric Constant on the Absorption of a Solvent-Exposed Nitrile Vibrational Stark Effect Probe

In these studies, we describe the systematic investigation of the effect of solvent dielectric changes on electrostatic fields at the protein-solvent interface using Vibrational Stark effect (VSE) spectroscopy and molecular dynamics (MD).[45] The thiocyanate (SCN) VSE spectral probe was incorporated at nine locations at the RalGDS-solvent interface: I18, R20, N27, G28, N29, Y31, K32, S33 and N54. The SCN-probe locations are highlighted in Figure 5.1. Six of the nine locations (N27, G28, N29, Y31, K32, and N54) are the same locations mentioned in Chapter 3.[17] All nine locations are included in the studies discussed in Chapter 4.[44] As previously mentioned, these locations were chosen based on a prior study that demonstrated a correlation between the absorption energy of the SCN probes and the solvent-accessible surface area (SASA).[6] Additionally, three small organic molecules with SCN functional groups – methyl thiocyanate (MeSCN) ethyl thiocyanate (EtSCN) and hexyl thiocyanate (HxSCN) – were chosen to investigate the effects of the solvent on the SCN probe without the complication of the protein system.

The SCN-spectral probes on three organic small molecules and nine locations on Ralβ were exposed to solvents with varying dielectrics through the controlled addition of glycerol to the solvent (0%, 10%, 20%, 30% and 40%). The absorption energies of each SCN probe were recorded in each solvent condition; the 0% absorption energy data for the SCN-labeled Ralβ locations were taken from a previous study.[6] We examined the ability of the Onsager solvation model to describe the changes in absorption energy of the SCN probes from the dielectric of the solvent. The absolute value of the Onsager factor, $|\Phi|$, for each solvent condition (0%, 10%, 20%, 30%, and 40%) was determined using
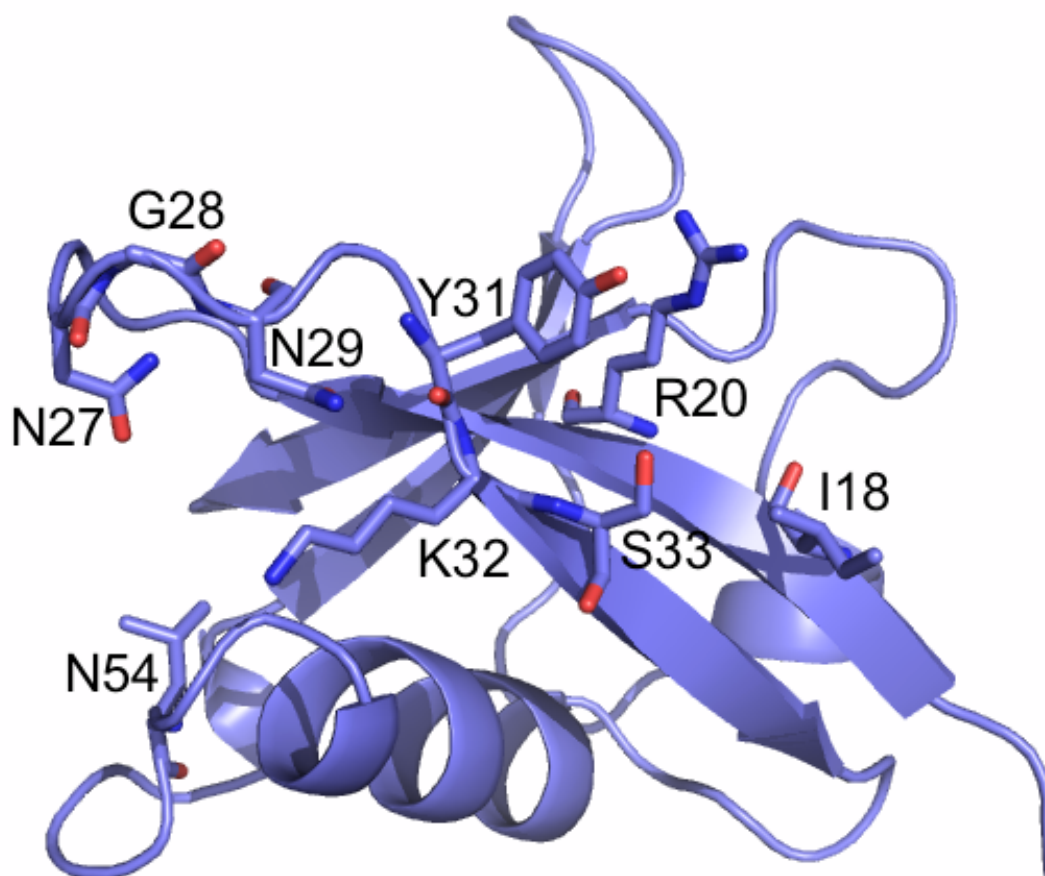
Figure 5. 1. A cartoon representation of Ral from 1LFD[29] highlighting the nine protein-solvent interfacial positions that were selected to incorporate the thiocyanate VSE spectral probe in this study.

Equation 1.2 to be 1.3797, 1.3784, 1.3770, 1.3754, and 1.3736 for a solute with n = 1.5. For each SCN probe, the absorption energies were strongly correlated with |Φ|. The solvent-induced changes on the absorption energies may be described by the simple Onsager model.

To understand the effects of local structure on the results of the Onsager model, Mr. Andrew Ritchie preformed molecular dynamics (MD) sampling of the SCN probe at each of the nine positions along Ralβ to create a Boltzmann-weighted statistical sample of low energy orientations of the SCN probe during the course of a steady-state experiment. From this data, we investigated several structural parameters such as the SCN probe's solvent-accessible surface area (SASA), elevation angle with respect to the protein-solvent surface, and extent of hydrogen bonding. None of these structural factors were found to correspond to the quality of the predictive ability of the absolute value of the Onsager model. However, SASA was found to inversely correlate with the ν *versus* |Φ| slope. According to Equation 1.3, the ν *versus* |Φ| slope is a function related to the inverse of the cavity radius cubed, $1/a^3$. The absolute value of the slope is expected to decrease as the radius of the cavity increases. This pattern held for the relationship of SASA to the ν *versus* |Φ| slope, which qualitatively demonstrated SASA to be related to a. We discuss reasons for the apparent generality of this simple model, even to complex cases of solvent-solute interactions.

5.1 VIBRATIONAL STARK EFFECT SPECTROSCOPY

5.1.1 Model Compounds

We were interested in testing the extent to which a SCN-probe sitting at the protein-water interface would have its local electrostatic environment changed

exclusively by changes in the magnitude of the solvent's reaction field. In this experiment, the electrochromic effect on the nitrile oscillator is caused only by changes in the extent of polarizability of the solvent, reported as its dielectric constant. Any significant deviation away from the model reaction field would indicate chemical effects such as hydrogen-bonding to the nitrile probe, a particular concern in a protic solvent. To test the utility of this analysis, the absorption energies of the VSE spectral probe, SCN probe, on three organic molecules – methyl thiocyanate (MeSCN), ethyl thiocyanate (EtSCN), and hexyl thiocyanate (HxSCN) – were measured as the dielectric constant of the aqueous solvent was lowered by adding glycerol. One mM solutions of the small molecule model compounds were dissolved in labeling buffer containing 0%, 10%, 20%, 30% and 40% glycerol, with dielectric constants of 80.37, 77.55, 74.72, 71.77 and 68.76, respectively.[36] The absorption energies and full-width half maximum (fwhm) are tabulated in Table 5.1, and representative spectra for MeSCN are shown in Figure 5.2. In all cases, as the glycerol content was increased from 0 to 40%, the absorption energy of the nitrile probe in these three thicyanate-containing alkanes decreased by ~1.0 cm^{-1}, while the fwhm increased by ~2.0 cm^{-1}. The small molecules, MeSCN and EtSCN, have refractive indices of 1.469[46] and 1.462,[47] respectively, and so $n = 1.5$ was estimated for all small molecules and Ral-based SCN probes in this analysis. The ability for the Onsager solvation model to explain the observed changes in absorption energies was examined by comparing the SCN absorption energies (v) from the model organic compounds to |Φ| for each glycerol concentration. The absorption energies (v) and |Φ| were found to be highly correlated, with $r = 1.0$, 0.92 and 0.99 for MeSCN, EtSCN and HxSCN, respectively, and with similar slopes and intercepts (Figure 5.3 and Table 5.2). This high correlation suggests that the Onsager model is able to describe the solvatochromic response of small

Table 5.1. Measured absorption frequencies ν_{obs} (cm^{-1}) and full-width half maximum (fwhm, cm^{-1}) of the SCN-labeled Ralβ mutants in labeling buffer with 0%, 10%, 20%, 30% or 40% glycerol (dielectric, ε, of the solvent); correlation constant of the fit (r) of the Onsager factor |Φ| *versus* ν_{obs}. Error is reported as one standard deviation from multiple experiments.

Ralβ Mutant		% Glycerol (ε)					
		0 (80.37)	10 (77.55)	20 (74.72)	30 (71.77)	40 (68.76)	r
I18C	ν_{obs} (cm^{-1})	2163.3 ± 0.2	2162.6 ± 0.2	2162.8 ± 0.1	2162.3 ± 0.1	2161.6 ± 0.4	0.937
	fwhm (cm^{-1})	13.2 ± 0.9	13.1 ± 0.7	13.3 ± 0.1	13.9 ± 0.3	15.7 ± 0.4	
R20C	ν_{obs} (cm^{-1})	2162.4 ± 0.1	2161.8 ± 0.1	2160.9 ± 0.2	2160.7 ± 0.3	2161.2 ± 0.1	0.759
	fwhm (cm^{-1})	13.7 ± 0.5	13.6 ± 0.3	14.4 ± 0.8	14.8 ± 0.7	15.1 ± 0.1	
N27C	ν_{obs} (cm^{-1})	2163.0 ± 0.3	2162.8 ± 0.3	2162.4 ± 0.1	2162.7 ± 0.3	2162.3 ± 0.2	0.814
	fwhm (cm^{-1})	13.2 ± 1.4	13.1 ± 0.2	13.4 ± 0.8	14.6 ± 0.9	15.9 ± 0.4	
G28C	ν_{obs} (cm^{-1})	2160.1 ± 0.1	2160.1 ± 0.2	2159.6 ± 0.1	2159.4 ± 0.1	2159.2 ± 0.2	0.966
	fwhm (cm^{-1})	15.3 ± 0.4	15.2 ± 0.8	16.6 ± 1.2	15.9 ± 0.4	19.7 ± 0.2	
N29C	ν_{obs} (cm^{-1})	2161.5 ± 0.2	2161.4 ± 0.2	2161.3 ± 0.1	2160.8 ± 0.3	2159.6 ± 0.1	0.911
	fwhm (cm^{-1})	14.3 ± 0.6	13.7 ± 1.0	15.0 ± 0.2	14.1 ± 0.8	18.1 ± 0.7	
Y31C	ν_{obs} (cm^{-1})	2161.6 ± 0.3	2161.3 ± 0.1	2161.1 ± 0.1	2160.9 ± 0.1	2160.6 ± 0.1	0.946
	fwhm (cm^{-1})	13.7 ± 0.3	14.1 ± 0.2	14.5 ± 0.1	14.6 ± 0.3	15.0 ± 0.4	
K32C	ν_{obs} (cm^{-1})	2160.7 ± 1.0	2160.4 ± 0.3	2160.0 ± 0.1	2159.2 ± 0.3	2159.0 ± 0.1	0.982
	fwhm (cm^{-1})	15.8 ± 0.9	15.2 ± 3.1	16.9 ± 0.7	14.8 ± 0.7	15.1 ±0.8	
S33C	ν_{obs} (cm^{-1})	2161.8 ± 0.4	2162.5 ± 0.2	2161.3 ± 0.2	2161.6 ± 0.2	2160.3 ± 0.2	0.631
	fwhm (cm^{-1})	14.9 ± 1.0	16.1 ±0.8	15.8 ± 0.4	15.8 ± 0.5	16.9 ± 0.1	
N54C	ν_{obs} (cm^{-1})	2162.2 ± 0.1	2162.3 ± 0.2	2161.7 ± 0.1	2162.0 ± 0.1	2161.3 ± 0.4	0.829
	fwhm (cm^{-1})	12.7 ± 0.4	12.8 ± 0.1	13.3 ± 0.2	13.1 ± 0.7	14.4 ± 0.1	
Model Compound							
MeSCN	ν_{obs} (cm^{-1})	2162.4 ± 0.1	2162.2 ± 0.1	2162.0 ± 0.1	2161.7 ± 0.1	2161.4 ±0.1	0.999
	fwhm (cm^{-1})	10.1 ± 0.1	10.7 ± 0.1	11.1 ± 0.1	11.9 ± 0.1	12.2 ± 0.1	
EtSCN	ν_{obs} (cm^{-1})	2159.9 ± 0.1	2159.6 ± 0.1	2159.8 ± 0.1	2159.1 ± 0.1	2158.8 ± 0.1	0.918
	fwhm (cm^{-1})	10.1 ± 0.1	10.7 ± 0.1	11.2 ± 0.1	11.9 ± 0.1	12.2 ± 0.1	
HxSCN	ν_{obs} (cm^{-1})	2159.0 ± 0.1	2158.8 ± 0.1	2158.4 ± 0.1	2158.2 ± 0.1	2158.0 ± 0.1	0.985
	fwhm (cm^{-1})	10.7 ± 0.1	10.5 ± 0.8	12.2 ± 0.4	12.3 ± 0.1	13.1 ± 0.1	
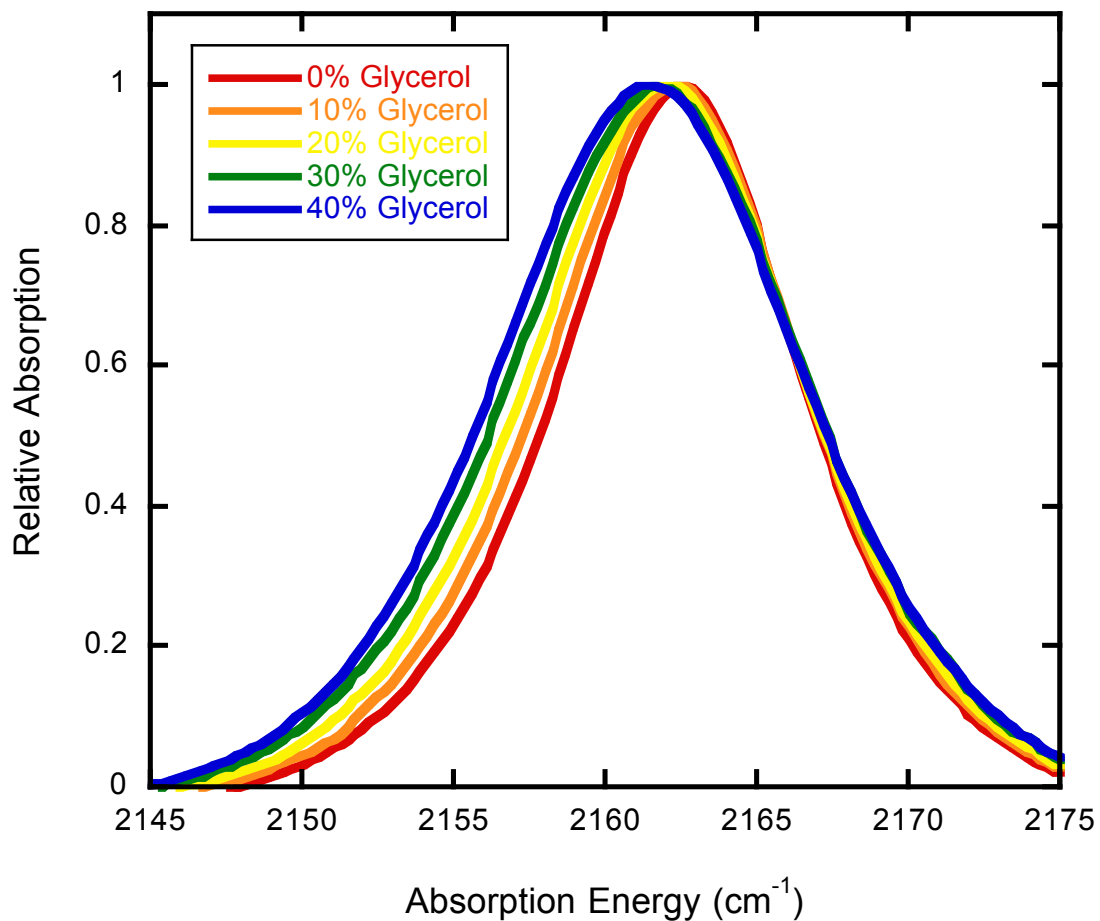
Figure 5.2.   Normalized, fitted absorbance of the thiocyanate on MeSCN measured in labeling buffer with 0% (red, 2162.4 cm^{-1}), 10% (orange, 2162.2 cm^{-1}), 20% (yellow, 2162.0 cm^{-1}), 30% (green, 2161.7 cm^{-1}) and 40% (blue, 2161.4 cm^{-1}) glycerol.
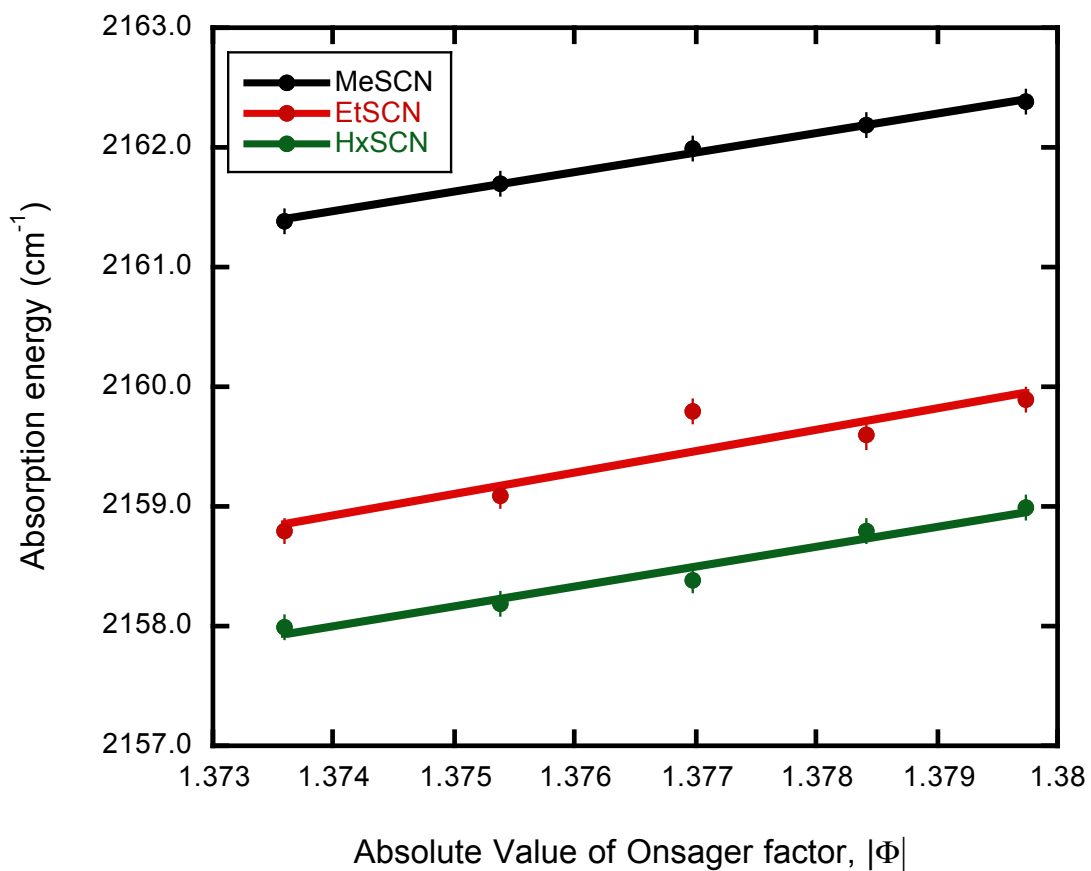
Figure 5.3. The absorption energies of MeSCN (black, $r = 1.0$), EtSCN (red, $r = 0.92$) and HxSCN (green, $r = 0.98$) compared to the response of MeSCN to the absolute value of the Onsager factor, $|\Phi|$. The vertical error bars indicate the standard deviation of the absorption energy.

molecules; however, the direction of the change of SCN absorption energy of the model compounds *versus* Φ is in the opposite direction to that which has been seen before for phenyl-based nitrile probes in aprotic solvents.[34,48,49] Experiments are underway in the laboratory to further examine the ability of the Onsager to describe the solvent induced vibrational shifts of the model molecules in a variety of solvents.

5.1.2 Nitrile Probes on the Surface of Ralβ

Next, we focused on the reaction field established around nitrile probes along a model protein-solvent interface. The nine locations of the nitrile probe investigated here are all solvent accessible (confirmed through our labeling chemistry), but sit in potentially dramatically different chemical and structural environments based on the local conformations of the protein's three-dimensional surface around each nitrile probe shown in Figure 5.1. Infrared spectra were taken and the absorption energies and the fwhm for the nine probe locations on Ralβ were recorded for solvent conditions containing 10, 20, 30 and 40% glycerol; these values were compared with energies and fwhm for 0% from a previous study shown in Table 5.1.[6] Each spectrum was processed with an in-house fitting program to find the peak center and fwhm; a minimum of four spectra was collected to obtain standard deviations. Representative spectra for Ralβ I18C$_{SCN}$ are shown in Figure 5.4. Identically to what was observed in the model compounds, that absorption energy of Ralβ I18C$_{SCN}$ decreased and the fwhm increased as the content of glycerol increased from 0 to 40%.

A similar trend was observed for all of the Ralβ probe locations, and is detailed in Table 5.1. Each Ralβ nitrile probe experienced a decrease in absorption energy as the dielectric constant of the solvent decreased. Figure 5.5 shows the absorption energy (v)

Table 5. 2.   The slope and y-intercepts from the Onsager factor |Φ| *versus* ν_{obs} and the Boltzmann-weighted SASA, elevation angle and frequency of H-bonding for the thiocyanate probe. Error is propagated from the least-squares fit of ν_{obs} for the slope and y-intercept. Standard deviation is derived from the Boltzmann-weighted distribution for SASA, elevation angle and H-bonding.

Ralβ Mutant	Slope	y-intercept	SASA ($\mathrm{\AA^2}$)	Elevation Angle	H-Bonding
I18C	243.57	1827.2	33 ± 12	12 ± 11	0.08 ± 0.27
R20C	217.90	1861.4	46 ± 8	47 ± 1	0.13 ± 0.33
N27C	96.68	2029.5	52 ± 30	20 ± 9	0.12 ± 0.32
G28C	162.89	1935.4	89 ± 13	1 ± 13	0.12 ± 0.33
N29C	295.18	1754.5	27 ± 14	-47 ± 10	0.03 ± 0.17
Y31C	195.91	1891.3	65 ± 15	19 ± 6	0.13 ± 0.34
K32C	299.93	1746.9	37 ± 14	49 ± 3	0.11 ± 0.31
S33C	275.71	1781.8	79 ± 19	28 ± 9	0.13 ± 0.34
N54C	138.91	1970.6	78 ± 13	27 ± 5	0.15 ± 0.36
Model Compound					
MeSCN	163.73	1936.5	130	N/A	N/A
ETSCN	178.86	1913.2	123	N/A	N/A
HxSCN	168.49	1926.5	129	N/A	N/A

Figure 5.4. Normalized, fitted absorbance of the thiocyanate on Ralβ I18C$_{SCN}$ measured in labeling buffer with 0% (red, 2163.3 cm^{-1}), 10% (orange, 2162.6 cm^{-1}), 20% (yellow, 2162.8 cm^{-1}), 30% (green, 2162.3 cm^{-1}) and 40% (blue, 2161.6 cm^{-1}) glycerol.
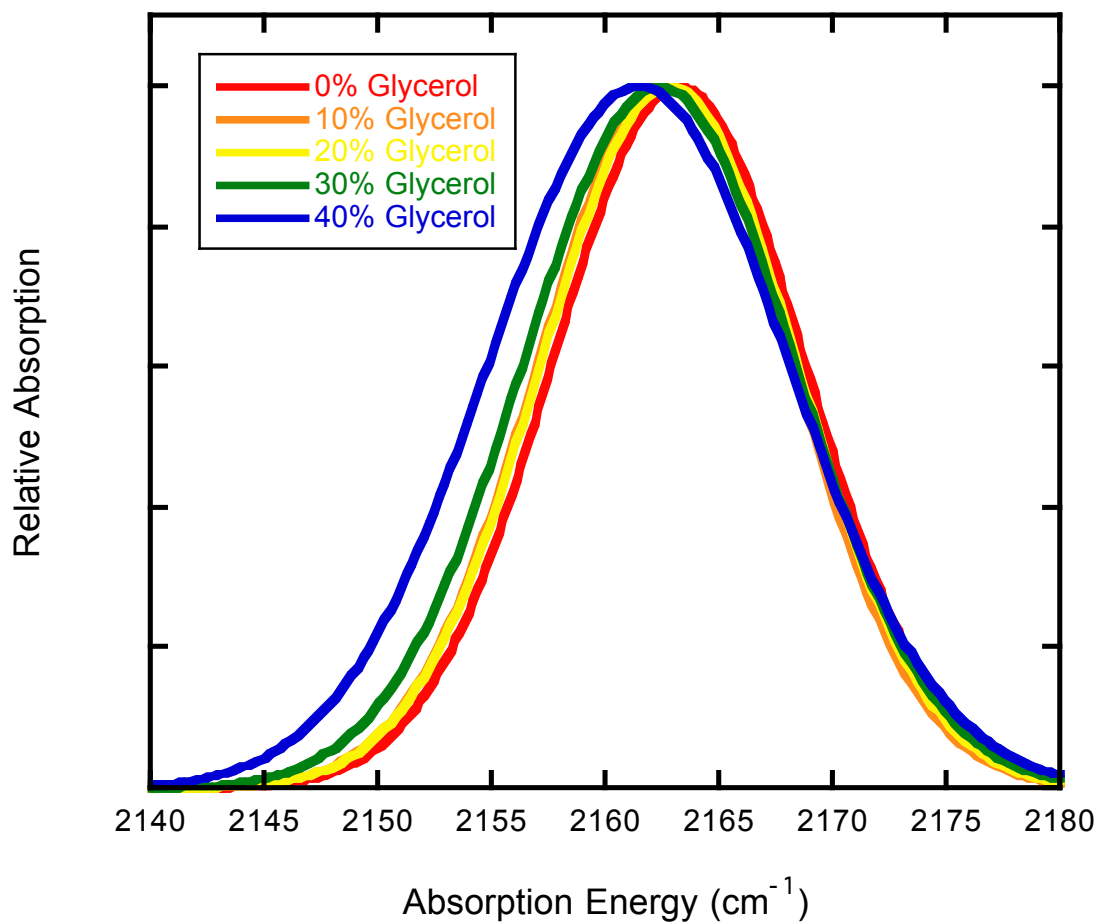
versus |Φ| of Ralβ I18C$_{SCN}$, Ralβ G28C$_{SCN}$ and MeSCN. In contrast to the three model compounds, the slopes and intercepts of each change in absorption energy (*v*) *versus* |Φ| varied widely based on the location of the probe along Ralβ's three-dimensional surface (Table 5.2). Differences in slopes are particularly interesting because they are directly related to the probe's ground state dipole moment, $\Delta\vec{\mu}$, and inversely proportional to the size of the solvent cavity surrounding the nitrile, a^3. The radius of the solvent cavity is obviously difficult to determine for even a simple diatomic oscillator like a nitrile probe, but can be estimated from structural parameters determined through molecular dynamics simulations.

5.2 MOLECULAR DYNAMICS SIMULATIONS

The ability of the Onsager model to describe a nitrile sitting at a protein-solvent (low dielectric – high dielectric) interface as well as a small molecule entirely solvated by a single dielectric continuum is surprising. The Onsager model has been used to model a variety of systems including the temperature dependence of vibrational frequences;[50] orientation in liquid crystal systems;[50] and structure and optical properties of dyes.[51] We were interested if certain structural parameters of the probe such as the extent of its exposure to water or hydrogen bonding to the solvent corresponded to the degree to which the Onsager model described its solvatochromic response. To investigate this, Mr. Andrew Ritchie from the Webb group performed extensive MD sampling to get a Boltzmann-weighted ensemble of orientations of the nitrile probe at the protein-solvent interface. Although these simulations have been carried out in an explicit solvent of tip3p water that did not contain any glycerol, because of the infrequency of water-nitrile hydrogen-bonding (<15% of all frames, shown in Table 5.2 and discussed further below),

74
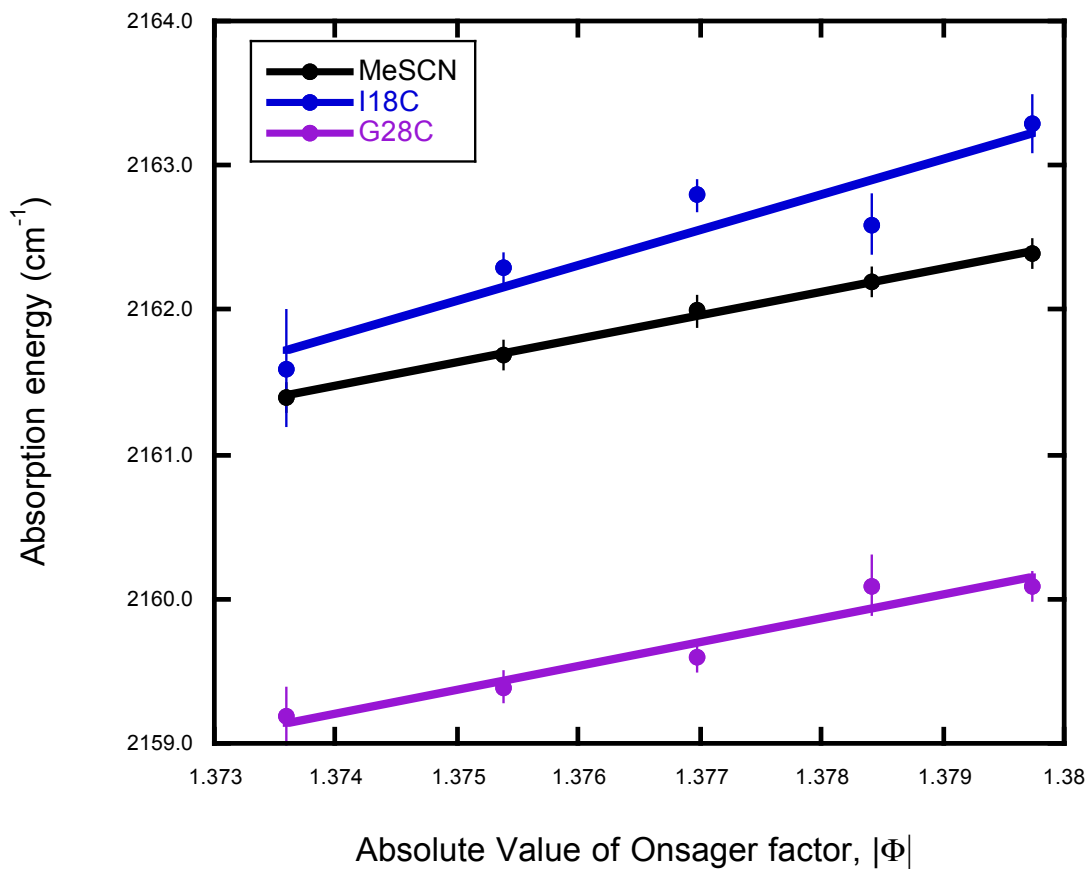
Figure 5.5. The absorption energies of MeSCN (black, $r = 1.0$), Ralβ I18C$_{SCN}$ (blue, $r = 0.94$) and Ralβ G28C$_{SCN}$ (purple, $r = 0.97$) compared to the response of MeSCN to the absolute value of the Onsager factor, $|\Phi|$. The vertical error bars indicate the standard deviation of the absorption energy.

side-chain steric interactions are the primary determinant of any deviations from akyl-like behavior. Because of this, we are confident that nitrile orientations obtained from simulating in 100% water are sufficient for our purposes.

Mr. Ritchie used the weighted-histogram analysis method (WHAM)[43] to derive dihedral torsional distributions of the χ_1 (N-Cα-Cβ-Sγ) and χ_2 (Cα-Cβ-Sγ-Cδ) dihedral angles of each nitrile probe. The torsional distributions are shown in Figure 5.6. For six of the nine probe locations, the probabilities were found to be alkane-like as expected, with the high probability of both torsion angles assuming values of ±60˚ and 180˚. For the remaining three probe locations, Ralβ R20C$_{SCN}$, Ralβ N29C$_{SCN}$ and Ralβ K32C$_{SCN}$, the calculated probabilities were observed to have fewer populated geometries, and further evaluation of the individual MD frames indicated that the probe was unable to occupy several of the expected alkane-like positions due to steric hindrances from other parts of the protein. Thus, although some structures are less alkane-like than would be expected for a completely unhindered probe, these results represent an accurate statistical ensemble of the probe orientations along χ_1 and χ_2.

The connection between our torsional distributions and the orientation of the probe within the protein was analyzed by defining a surface "elevation angle," which is the angle between the nitrile Cδ–Nϵ vector and a plane defined by a vector normal to the protein backbone center-of-mass to the nitrile Cα, called the surface plane. Both the normal vector and the angle were computed using a script developed in-house and were combined with the WHAM probabilities to find the average angle of elevation for each probe in the system. These angles and their variances are tabulated in Table 5.2, where an angle of 0˚ indicates a probe that is parallel to the protein-water interface, angles >0 are pointing out into solvent, and angles <0 are pointing back towards the protein. Six of

Figure 5.6. Torsional distributions of the χ_1 and χ_2 angles of each of the 9 SCN-probe Ralβ locations from WHAM, where the probability of a particular combination of χ_1 and χ_2 angles increases as the color moves from black to blue to cyan. Six of the mutants have high probabilities of being located at χ_1 and χ_2 angles of 60, -60 and 180 degrees, as expected for alkanes. Three of the probe locations, Ralβ R20C, N29C and K32C have one or more of the alkane expected probabilities suppressed. Data and figure prepared by Mr. Ritchie.

the Ralβ probe positions, I18C$_{SCN}$, N27C$_{SCN}$, G28C$_{SCN}$ Y31C$_{SCN}$, S33C$_{SCN}$, and N54C$_{SCN}$ were approximately parallel to the protein-water surface with angles ranging from 0˚ to 30˚. Two of the probe locations, R30C and K32C, were pointed further away from the protein, between 45˚ and 50˚. Ralβ N29C$_{SCN}$ is the only probe in the set in which the probe is actually pointing back in towards the protein at an angle of 45˚.

To quantify the hydration of the probe, Mr. Ritchie calculated the Boltzmann-weighted solvent-accessible surface area (SASA) of the sulfur, carbon, and nitrogen atoms for each probe location using the built in function g_sas from GROMACS with a defined radius of 1.4 Å. The WHAM probability distributions were combined with the individual SASAs from each from to create Boltzmann-weighted distributions for SASA shown in Table 5.2. The measured SASA for the SCN probe on MeSCN was found to be 130 Å^2 and did not vary significantly by lengthening the alkyl chain. In contrast, measured SASAs for each Ralβ probes were significantly smaller and more variable, ranging from Ralβ N29C$_{SCN}$ with 27 Å^2 to Ralβ S33C$_{SCN}$ with 79 Å^2. Our quantitative structural modeling of each nitrile location revealed very different solvent environments around each of these probes, and yet VSE measurement showed they all responded similarly to changes in solvent polarizability according to a simple Onsager analysis. This in turn implies that a simple Onsager model may be appropriate even for changes in absorption energy for a probe in a variety of positions along a protein-solvent interface, and that it is a simple reporter of its immediate electrostatic environment.

Furthermore, although there is no correlation between SASA and elevation angle, there is a correlation between SASA and both slope and intercept of ν *versus* |Φ|; Figure 5.7 shows that as SASA increases, the slope of ν *versus* |Φ| decreases. Equation 1.3 shows that the slope of ν *versus* |Φ| is dependent on two constants for the nitrile, the

Stark tuning rate, $\Delta\vec{\mu}$, and the dipole moment, $\vec{\mu}_0$, as well as a, the radius of the cavity. As a increases and the volume of the solvent cavity increases the magnitude of the slope decrease. Qualitatively, this result indicates that a and SASA are correlated, which makes intuitive sense as both a and SASA are related to the size of the cavity taken up by the SCN-probe.

There were several significant outliers to this trend, most noticeably Ralβ N27C$_{SCN}$, and Ralβ S33C$_{SCN}$. These two probes did not have unusual values of SASA or elevation angle, and so structurally did not seem to be different from the other Ralβ probes in any significant way. However, an additional reason the measured slope or intercept could be significantly different from the Onsager model, which assumes that the interaction between solute and solvent is based purely through the induced reaction field, is if there are significant effects changing the absorption energy of the probe that are convoluted into the measurement of ν_{obs}. One possibility that has been extensively discussed in the context of nitrile probes is hydrogen bonding between the nitrile and the solvent. Our laboratory has recently demonstrated how the kinds of MD simulations described here can be used to quantify the extent and effect of hydrogen-bonding to the nitrile.[52] Therefore, Mr. Ritchie used MD simulations to quantify the number and frequency of hydrogen bonds to the nitrile at each probe location on the Ralβ monomers. To avoid undercounting potential hydrogen bonds, we used generous criteria to define the presence of a hydrogen bond, setting the distance between the nitrile nitrogen atom and solvent hydrogen of ≤ 2.25 Å and the angle between the nitrile nitrogen atom and the solvent H-O group at $\geq 138°$.[53] These parameters were used to count the number of hydrogen bonds in each frame of the MD simulation; this data was then Boltzmann-weighted from the WHAM distribution. This analysis revealed that hydrogen bonding to
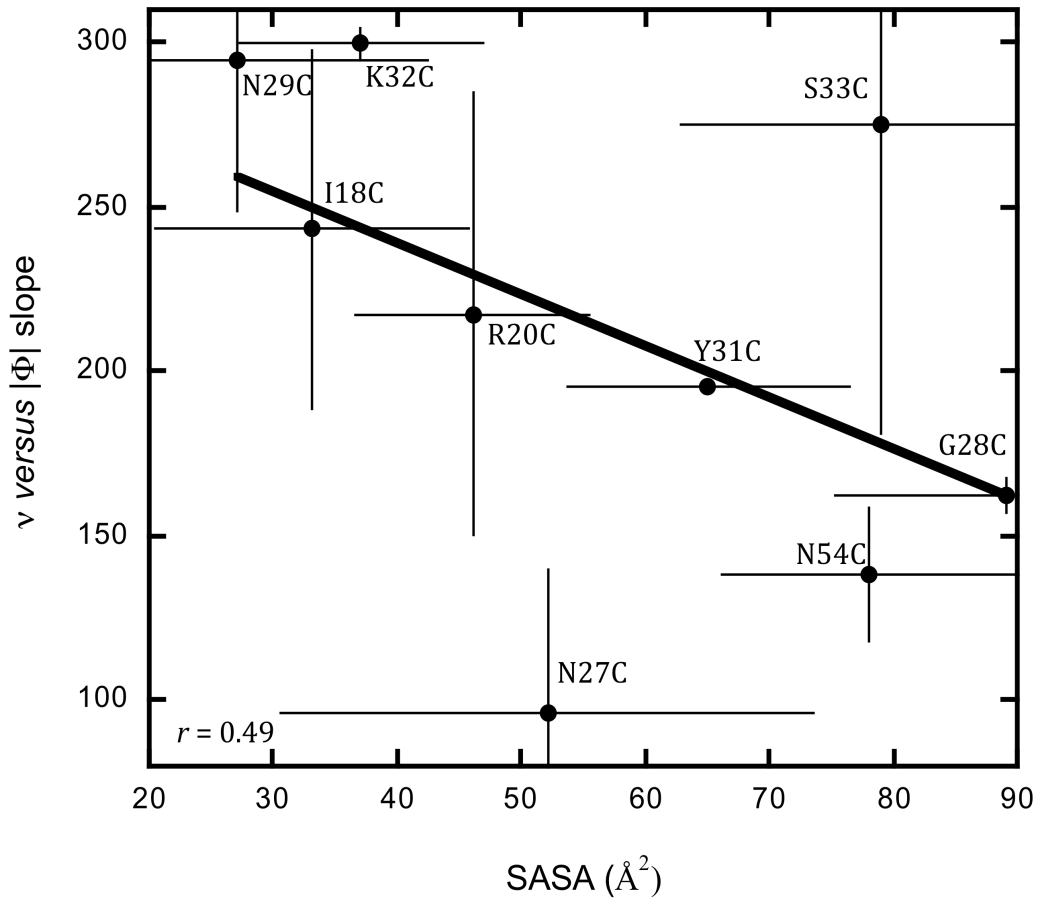
Figure 5.7. The slopes from the ν *versus* |Φ| comparisons compared to the calculated SASA for each of the SCN-labeled Ralβ locations. The horizontal error bars indicate the standard deviation of the SASA measurement. The vertical error bars are the propagated error from the ν *versus* |Φ| comparisons.

the nitrile nitrogen atom was an infrequent event for all locations of the nitrile probe, with < 15% of any simulation frame containing a single hydrogen bond. Ralβ $N27C_{SCN}$ and $S33C_{SCN}$ displayed one hydrogen bond in 12% and 13% of the simulation frames, respectively, and while this was the high end of what was observed, it was less than the number of hydrogen bonds observed at $R20C_{SCN}$ (13%) or $N54C_{SCN}$ (15%). Furthermore, both of these mutants displayed the expected alkane-like structure of the thiocyanate side chain described above. This may indicate the limit of an Onsager-type analysis on a real protein, although does not detract from the overall observation of that this model may describe the reaction field in a non-spherical environment.

5.3 CONCLUSIONS

The absorption energy of a solvent exposed SCN-spectral probe on 3 model compounds and 9 locations on RalGDS was observed to be sensitive to the polarizability of the solvent, described by the solvent's dielectric constant. The Onsager reaction field solvation model may be able to describe this sensitivity despite the model's lack of molecular-level details. In the Onsager model, a self-constant field is created by the polarization of solvent when a molecule with a dipole moment, $\vec{\mu}_0$, is placed into the solvent. The absorption energy (ν) of the SCN probe in 3 organic molecules and 9 locations of the RalGDS interface was found to correlate with the calculated absolute value of the Onsager factor ($|\Phi|$), the part of the reaction field described by the polarizability of the solvent and the SCN-probe. The direction of the ν versus Φ was opposite to previous studies; therefore, studies are underway to investigate several more solvents. Several physical characteristics of the SCN probes on the RalGDS surface were simulated including the solvent assessable solvent area (SASA), the angle of the probe at

the interface and the frequency of hydrogen bonding to the SCN probe. No correlation was found between the physical characteristics of the SCN probe and the ability of the Onsager model to describe the observed solvent shift for each probe; however, the slope of the absorption energy, v, *versus* Onsager factor, $|\Phi|$, was found to correlate with the probe's SASA. This result is not surprising as the slope is dependent of a, the radius of the cavity occupied by the probe. The observed reliance SASA for the amount the absorption energy changes due to the change in the Onsager factor suggests that SASA correlates with a.

Bibliography

(1)   Lee, L. P.; Tidor, B."Optimization of Binding Electrostatics: Charge Complementarity in the Barnase-Barstar Protein Complex" *Protein Science* **2001**, *10*, 362-377.

(2)   Honig, B.; Nicholls, A."Classical Electrostatics in Biology and Chemistry" *Science* **1995**, *268*, 1144-1149.

(3)   Villa, J.; Warshel, A."Energetics and Dynamics of Enzymatic Reactions" *J. Phys. Chem. B* **2001**, *105*, 7887-7907.

(4)   Webb, L. J.; Boxer, S. G."Electrostatic Fields Near the Active Site of Human Aldose Reductase: 1. New Inhibitors and Vibrational Stark Effect Measurements" *Biochemistry* **2008**, *47*, 1588-1598.

(5)   Fafarman, A. T.; Webb, L. J.; Chuang, J. I.; Boxer, S. G."Site-Specific Conversion of Cysteine Thiols into Thiocyanate Creates an IR Probe for Electric Fields in Proteins" *J. Am. Chem. Soc.* **2006**, *128*, 13356-13357.

(6)   Stafford, A. J.; Ensign, D. L.; Webb, L. J."Vibrational Stark Effect Spectroscopy at the Interface of Ras and Rap1A Bound to the Ras Binding Domain of RalGDS Reveals an Electrostatic Mechanism for Protein-Protein Interaction" *J. Phys. Chem. B* **2010**, *114*, 15331-15344.

(7)   Klotz, I. M."Protein Hydration and Behavior" *Science* **1958**, *128*, 815-822.

(8)   Bryant, R. G.; Shirley, W. M."Dynamical deductions from nuclear magnetic resonance relaxation measurements at the water-protein interface" *Biophys. J.* **1980**, *32*, 3-16.

(9)   Warshel, A.; Russell, S. T."Calculations of electrostatic interactions in biological systems and in solutions" *Q Rev Biophys* **1984**, *17*, 283-422.

(10)   Warshel, A.; Sharma, P. K.; Kato, M.; Parson, W. W."Modeling electrostatic effects in proteins" *Biochim. Biophys. Acta* **2006**, *1764*, 1647-1676.

(11)   Ren, P.; Chun, J.; Thomas, D. G.; Schnieders, M. J.; Marucho, M.; Zhang, J.; Baker, N. A."Biomolecular electrostatics and solvation: a computational perspective" *Q Rev Biophys* **2012**, *45*, 427-491.

(12)   Forsyth, W. R.; Antosiewicz, J. M.; Robertson, A. D."Empirical Relationships Between Protein Structure and Carboxyl pKa Values in Proteins" *Proteins* **2002**, *48*, 388-403.

(13)   Schutz, C. N.; Warshel, A."What are Dielectric "Constants" of Proteins and How to Validate Electrostatic Models?" *Proteins* **2001**, *44*, 400-417.

(14)   Tanford, C.; Kirkwood, J. G."Theory of Protein Titration Curves. I. General Equations for Impenetrable Spheres" *J. Am. Chem. Soc.* **1957**, *79*, 5333-5339.

(15)   Danielson, M. A.; Falke, J. J."Use of 19F NMR To Probe Protein Structure and Conformational Changes" *Annu. Rev. Biophys. Biomol. Struct.* **1996**, *25*, 163-195.

(16)   Pearson, J. G.; Oldfield, E.; Lee, F. S.; Warshel, A."Chemical Shifts in Proteins: A Shielding Trajectory Analysis of the Fluorine Nuclear Magnetic Resonance Spectrum of the Escherichia coli Galactose Binding Protein Using a Multipole Shielding Polarizability-Local Reaction Field-Molecular Dynamics Approach" *J. Am. Chem. Soc.* **1993**, *115*, 6851-6862.

(17)   Ragain, C. M.; Newberry, R. W.; Ritchie, A. W.; Webb, L. J."Role of Electrostatics in Differential Binding of RaIGDS to Rap Mutations E30D and K31E Investigated by Vibrational Spectroscopy of Thiocyanate Probes" *J. Phys. Chem. B.* **2012**, *116*, 9326-9336.

(18)   Stafford, A. J.; Walker, D. M.; Webb, L. J."Electrostatic Effects of Mutations of Ras Glutamine 61 Measured Using Vibrational Spectroscopy of a Thiocyanate Probe" *Biochemistry* **2012**, *51*, 2757-2767.

(19)   Park, E. S.; Andrews, S. S.; Hu, R. B.; Boxer, S. G."Vibrational Stark Spectroscopy in Proteins: A Probe and Calibration for Electrostatic Fields" *J. Phys. Chem. B* **1999**, *103*, 9813-9817.

(20)   Andrews, S. S.; Boxer, S. G."Vibrational Stark Effects of Nitriles I. Methods and Experimental Results" *J. Phys. Chem. A* **2000**, *104*, 11853-11863.

(21)   Walker, D. M.; Hayes, E. C.; Webb, L. J."Vibrational Stark effect spectroscopy reveals complementary electrostatic fields created by protein-protein binding at the interface of Ras and Ral" *Phys Chem Chem Phys* **2013**, *15*, 12241-12252.

(22)   Krauss, G. *Biochemistry of Signal Transduction and Regulation*, 3 ed.; WILEY-VCH Verlag: Weinheim, Germany, 2003.

(23)   Nassar, N.; Horn, G.; Herrmann, C.; Scherer, A.; McCormick, F.; Wittinghofer, A."The 2.2 A crystal structure of the Ras-binding domain of the serine/threonine kinase c-Raf1 in complex with Rap1A and a GTP analogue" *Nature* **1995**, *375*, 554-560.

(24)   Cox, A. D.; Der, C. J."The dark side of Ras: regulation of apoptosis" *Oncogene* **2003**, *22*, 8999-9006.

(25)   Downward, J."Targeting Ras Signalling Pathways in Cancer Therapy" *Nature Canc. Rev.* **2002**, *3*, 11-22.

(26)   Repasky, G. A.; Chenette, E. J.; Der, C. J."Renewing the conspiracy theory debate: does Raf function alone to mediate Ras oncogenesis?" *Trends Cell Biol.* **2004**, *14*, 639-647.

(27)   Ahmed, S. M.; Daulat, A. M.; Meunier, A.; Angers, S."G Protein beta gamma Subunits Regulate Cell Adhesion through Rap1a and Its Effector Radil" *J. Biol. Chem.* **2010**, *285*, 6538-6551.

(28)   Bailey, C. L.; Kelly, P.; Casey, P. J."Activation of Rap1 promotes prostate cancer metastasis" *Cancer Res* **2009**, *69*, 4962-4968.

(29)   Huang, L.; Hofer, F.; Martin, G. S.; Kim, S. H."Structural basis for the interaction of Ras with RalGDS" *Nat. Struct. Biol.* **1998**, *5*, 422-426.

(30)   Nassar, N.; Horn, G.; Herrmann, C.; Block, C.; Janknecht, R.; Wittinghofer, A."Ras/Rap effector specificity determined by charge reversal" *Nat. Struct. Biol.* **1996**, *3*, 723-729.

(31)   Shirouzu, M.; Koide, H.; Fujitayoshigaki, J.; Oshio, H.; Toyama, Y.; Yamasaki, K.; Fuhrman, S. A.; Villafranca, E.; Yokoyama, S.; Kaziro, Y."Mutations That Abolish the Ability of Ha-Ras to Associate with Raf-1" *Oncogene* **1994**, *9*, 2153-2157.

(32)   Ensign, D. L.; Webb, L. J."Factors Determining Electrostatic Fields at the Ras/Effector Interface." *Proteins* **2011**, *79*, 3511-3524.

(33)   Onsager, L."Electric moments of molecules in liquids" *J. Am. Chem. Soc.* **1936**, *58*, 1486-1493.

(34)   Levinson, N. M.; Fried, S. D.; Boxer, S. G."Solvent-induced infrared frequency shifts in aromatic nitriles are quantitatively described by the vibrational Stark effect" *J Phys Chem B* **2012**, *116*, 10470-10476.

(35)   Kapust, R. B.; Tozser, J.; Fox, J. D.; Anderson, D. E.; Cherry, S.; Copeland, T. D.; Waugh, D. S."Tobacco etch virus protease: mechanism of autolysis and rational design of stable mutants with wild-type catalytic proficiency" *Protein Eng.* **2001**, *14*, 993-1000.

(36)   Akerlof, G."Dielectric constants of some organic solvent-water mixtures at various temperatures " *J. Am. Chem. Soc.* **1932**, *54*, 4125-4139.

(37)   Herrmann, C.; Horn, G.; Spaargaren, M.; Wittinghofer, A."Differential Interactions of the Ras Family of GTP-binding Proteins H-Ras, Rap1A, and R-Ras with the Putative Effector Meolecules Raf Kinase and Ral-Guanine Nucleotide Exchange Factor" *J. Biol. Chem.* **1996**, *271*, 6794-6800.

(38)   Schrödinger, L. The PyMOL Molecular Graphics System, Version 1.3r1, 2010.

(39)   Case, D. A.; Darden, T. A.; Cheatham, T. E.; Simmerling, C. L.; Wang, J.; Duke, R. E.; Luo, R.; Walker, R. C.; Zhang, W.; Merz, K. M. et al. *AMBER 11*; University of California, San Francisco, 2010.

(40)   Jorgensen, W. L.; Chandrasekhar, J.; Madura, J. D.; Impey, R. W.; Klein, M. L."Comparison of Simple Potential Functions for Simulating Liquid Water" *J. Chem. Phys.* **1983**, *79*, 926-935.

(41)   van der Spoel, D.; Lindahl, E.; Hess, B.; Groenhof, G.; Mark, A. E.; Berendsen, H. J. C."GROMACS: Fast, Flexible, and Free" *J. Comput. Chem.* **2005**, *26*, 1701-1718.

(42)   Roux, B."The calculation of the potential of mean force using computer simulations" *Comp. Phys. Commun.* **1995**, *91*, 275-282.

(43)   Gallicchio, E.; Andrec, M.; Felts, A. K.; Levy, R. M."Temperature Weighted Histogram Analysis Method, Replica Exchange, and Transition Paths" *J. Phys. Chem. B* **2005**, *109*, 6722-6731.

(44)   Ragain, C. M.; Ritchie, A. W.; Arrington, C. A.; Gonzalez, N. S.; Newberry, R. W.; Webb, L. J."Changes in Local Electrostatic Fields Caused by the Ras Mutations D30E and E31K Quantified by Vibrational Stark Effect Spectroscopy Create Rap-Like Docking to the Downstream Effector RalGDS" *In preparation.* **2014**.

(45)   Ragain, C. M.; Ritchie, A. W.; Gonzalez, N. S.; Newberry, R. W.; Rivas, J. N.; Webb, L. J."Solvent-Induced Changes in the Absorption of Vibrational Stark Effect Probes are Described by the Onsager Reaction Field at the Protein-Solvent Interface" *In preparation.* **2014**.

(46)   Chirico, R. D.; Frenkel, M.; Diky, V. V.; March, K. N.; Wilhoit, R. C."*J. Chem. Eng. Data* **2003**, *48*, 1344.

(47)   Diky, V.; Muzny, C. D.; Lemmon, E. W.; Chirico, R. D.; Frenkel, M."*J. Chem. Inf. Model.* **2009**, *49*, 503.

(48)   Elenewski, J. E.; C Hackett, J."Solvatochromism and the solvation structure of benzophenone" *J. Chem. Phys.* **2013**, *138*, -.

(49)   Aschaffenburg, D. J.; Moog, R. S."Probing Hydrogen Bonding Environments: Solvatochromic Effects on the CN Vibration of Benzonitrile" *J. Phys. Chem. B* **2009**, *113*, 12736-12743.

(50)   Kasyanenko, V. M.; Keiffer, P.; Rubtsov, I. V."Intramolecular vibrational coupling contribution to temperature dependence of vibrational mode frequencies" *J. Chem. Phys.* **2012**, *136*, -.

(51)   Wang, C.-K.; Xing, X.-J.; Huang, X.-M.; Gao, Y."Solvent effects on structure and optical properties of a D-π-A azobenzene dye" *Chin. Phys.* **2007**, *16*, 3323.

(52)   Ritchie, A. W.; Webb, L. J."Inclusion of Explicit Solvent Near a Vibrational Stark Probe Shows No Improvement Over Purely Implicit Solvent in the Calculation of Protein Electrostatic Field Changes Using APBS" *J. Phys. Chem. B.* **2013**, submitted.

(53)   Le Questel, J.-Y.; Berthelot, M.; Laurence, C."Hydrogen-bond acceptor properties of nitriles: a combined crystallographic and ab initio theoretical investigation" *J. Phys. Org. Chem.* **2000**, *13*, 347-358.

Vita

Christina Marie Ragain was born in Austin, TX and moved around the country during her childhood. Christina attended Oak Ridge High School in Oak Ridge, TN during which she spent her senior year as an exchange student to Germany through the Congress-Bundestag exchange program. Upon returning to the US, she began studying chemistry as an undergraduate at Maryville College in Maryville, TN. After 2 years, Christina transferred to the University of North Carolina at Greensboro where she worked with Dr. Liam Duffy in the Department of Chemistry. Christina completed her Master's of Science in Chemistry with Dr. J. Patrick Loria at Yale University. Christina spent 3 years teaching as a lecturer of chemistry at The University of Texas at Tyler before returning to graduate studies at The University of Texas at Austin to work with Dr. Lauren Webb.

Permanent email: cmragain@gmail.com

This dissertation was typed by Christina Ragain